Ionized and atomic interstellar medium in star-forming galaxies –

Thøger Emil Rivera-Thorsen

Ionized and atomic interstellar medium in star-forming galaxies

Thøger Emil Rivera-Thorsen

Cover image: 2D spectrum image of the Hα and surrounding [N II] lines of Haro 11 B, as treated in Paper II in this thesis. The horizontal axis shows wavelength, while the vertical axis shows spatial extent. The central horizontal line is the continuum trace of the hot, central star cluster. Around this, the stunningly complex line emission from the surrounding recombination nebula reveals intricate kinematics in high detail. Making physical sense of these patterns, and understanding what kind of conditions creates them, was the purpose of Paper II. The image was made from data obtained with the ESO X-Shooter spectrograph on the Very Large Telescope in Paranal, Chile, during the X-Shooter Science Verification Program in August 2009 under Program 60.A-9433(A), PI Göran Östlin.

ISBN 978-91-7649-545-2

Printed in Sweden by Holmbergs, Malmö 2016
Distributor: Department of Astronomy, Stockholm University

Til Eskil og Storm.

Elsk – og berig med drøm – alt stort som var.
Gå mod det ukendte, fravrist det svar!
Ubygde kraftværker, ukendte stjerner –
Skab dem, med skånet livs dristige hjerner.

— Nordahl Grieg, 1936

List of Papers

Included in thesis

These papers are referred to in the text by their roman numerals.

PAPER I: **The Lyα Reference Sample. I. Survey Outline and First Results for Markarian 259**
Östlin, G.; Hayes, M.; Duval, F.; Sandberg, A.; Rivera-Thorsen, T.; Marquart, T.; Orlitová, I. Adamo, A.; Melinder, J.; Guaita, L.; Atek, H.; Cannon, J. M.; Gruyters, P.; Herenz, E. C.; Kunth, D.; Laursen, P.; Mas-Hesse, J. M.; Micheva, G.; Otí-Floranes, H.; Pardy, S. A.; Roth, M. M.; Schaerer, D.; Verhamme, A.*The Astrophysical Journal*, **Volume 797, Issue 1, article id. 11**, 23pp (2014).
DOI: 10.1088/0004-637X/797/1/11

PAPER II: **The Lyman Alpha Reference Sample. V. The Impact of Neutral ISM Kinematics and Geometry on Lyα Escape**
Rivera-Thorsen, T. E.; Hayes, M.; Östlin, G.; Duval, F.; Orlitová, I.; Verhamme, A.; Mas-Hesse, J. M.; Schaerer, D.; Cannon, J. M.; Otí-Floranes, H.; Sandberg, A.; Guaita, L.; Adamo, A.; Atek, H.; Herenz, E. C.; Kunth, D.; Laursen, P.; Melinder, J., *The Astrophysical Journal*, **Volume 805, Issue 1, article id. 14**, 26 pp. (2015).
DOI: 10.1088/0004-637X/805/1/14

PAPER III: **Of Needles and Haystacks: Spatially Resolved Gas Kinematics in Starburst Galaxies Haro 11 and Eso 338 From Nuv/Optical Long-Slit Spectroscopy**
Rivera-Thorsen, T. E.; Östlin, G.; Bik, A.; Hayes, M.; Sandberg, A., *The Astrophysical Journal*, **submitted**.

PAPER IV: **The Lyman Continuum Escape and ISM properties in Tololo 1247-232 – New Insights from HST and VLA**

Puschnig, J.; Hayes, M.; Östlin, G.; Rivera-Thorsen, T E.; Melinder, J.; Cannon, J. M.; Menacho, V.; Zackrisson, E.; Bergvall, N.; Leitet, E. *Monthly Notices of The Royal Astronomical Society*, **submitted**.

PAPER V: **ISM, Lyman-alpha and Lyman-continuum in nearby starburst Haro 11**
Rivera-Thorsen, T. E.; Östlin, G.; Hayes, M.; Puschnig, J. *The Astrophysical Journal*, **draft**.

By the same author - not included in thesis

PAPER VI: **Galaxy counterparts of metal-rich damped Lyα absorbers - II. A solar-metallicity and dusty DLA at $z_{\rm abs} = 2.58$**
Fynbo, J. P. U. . . . (13 coauthors). . . Rivera-Thorsen, T. E. . . . (2 coauthors). *MNRAS*, **413.4**, 2481 (2011)
DOI: 10.1111/j.1365-2966.2011.18318.x

PAPER VII: **Neutral gas in Lyman-alpha emitting galaxies Haro 11 and ESO 338-IG04 measured through sodium absorption**
Sandberg, A. . . . (5 coauthors). . . Rivera-Thorsen, T. E. *A&A*, **552.A95**, 8 (2013)
DOI: 10.1051/0004-6361/201220702

PAPER VIII: **On the two high-metallicity DLAs at z = 2.412 and 2.583 towards Q 0918+1636**
Fynbo, J. P. U. . . . (9 coauthors). . . Rivera-Thorsen, T. E. . . . (1 coauthor). *MNRAS*, **436.1**, 361 (2013)
DOI: 10.1093/mnras/stt1579

PAPER IX: **Optical and near-IR observations of the faint and fast 2008ha-like supernova 2010ae**
Stritzinger, M. . . . (3 coauthors). . . Rivera-Thorsen, T. E. . . . (19 coauthor). *A&A*, **561.A146**, 22 (2014)
DOI: 10.1051/0004-6361/201322889

PAPER X: **The Lyman alpha reference sample. II. Hubble Space Telescope Imaging Results, Integrated Properties, and Trends**
Hayes, M. . . . (16 coauthors). . . Rivera-Thorsen, T. E. . . . (1 coauthor). *ApJ*, **782.1**, 22 (2014)
DOI: 10.1088/0004-637X/782/1/6

PAPER XI: **The Lyman alpha reference sample. III. Properties of the Neutral ISM from GBT and VLA Observations**
Pardy, S. . . . (3 coauthors). . . Rivera-Thorsen, T. E. . . . (14 coauthors). *ApJ*, **794.2**, 19 (2014)
DOI: 10.1088/0004-637X/794/2/101

PAPER XII: **The Lyman alpha reference sample. IV. Morphology at low and high redshift**
Guaita, L. . . . (16 coauthors). . . Rivera-Thorsen, T. E. . . . (6 coauthors). *A&A*, **576.A51**, 44 (2015)
DOI: 10.1051/0004-6361/201425053

PAPER XIII: **The Lyman alpha reference sample. VI. Lyman alpha escape from the edge-on disk galaxy Mrk 1486**
Duval, F. . . . (10 coauthors). . . Rivera-Thorsen, T. E. . . . (7 coauthors). *A&A*, **587.A77**, 24 (2016)
DOI: 10.1051/0004-6361/201526876

PAPER XIV: **The Lyman alpha reference sample. VII. Spatially resolved Hα kinematics**
Herenz, E. C. . . . (18 coauthors). . . Rivera-Thorsen, T. E.; . . . (2 coauthors). *A&A*, **587.A78**, 27 (2016)
DOI: 10.1051/0004-6361/201527373

Author's contribution to papers

Here follows a brief summary of my contributions to the papers included in this thesis.

PAPER I For this paper, I re-measured fluxes of nebular emission lines in the SDSS spectra of the LARS galaxies. From this, I computed improved redshifts for the galaxies, which were also used in Paper II, as well as metallicities, ionization parameters etc., tabularized in tables 1 and 2 in this paper. The fluxes also were used to place the sample galaxies in the BPT diagram of fig. 4, but I did not create this figure. The emission lines measurements of the SDSS spectra were also included in Hayes et al. (2014) (Paper X).

PAPER II I performed the analysis, created graphs and tables, and wrote the article apart from sect. 2.2, under guidance from my thesis advisors and taking suggestions from coauthors. I did *not* perform the data reduction described in sect. 2.2.

PAPER III I reduced the raw spectra, wrote the software package used for the analysis, performed the analysis, created figures and tables, and wrote the article under guidance from my thesis advisors and taking suggestions and advise from coauthors. The idea was fostered by G. Östlin and since developed further in collaboration.

PAPER IV For this paper, I performed a kinematic and Apparent Optical Depth analysis of metal absorption lines in the the FUV HST-COS spectrum of the target galaxy, and provided the values tabularized in table 2. I also created figs. 7, 8, 9, 10, and 11.

PAPER V I performed the analysis, created tables and figures and wrote the paper under guidance from my thesis supervisors and taking suggestions from co-authors. I did *not* reduce the data.

Part of the written material in this thesis, including Paper II, was also included in my Licentiate thesis (2015).

Contents

1. The Lyman α Universe

Lyman α (often abbreviated Lyα) is the transition of an electron between the ground state and the first excited state of neutral Hydrogen. The energy difference between these levels corresponds to the emission/absorption of a photon with a wavelength of $\lambda = 1215.67$ Ångström. Lyman α owes its importance to hydrogen being by far the most abundant element in the Universe. The sheer abundance of it means that any given photon has a much larger probability of encountering a Hydrogen atom than any other element. On cosmological distances, Lyα will often be the only emission strong enough to detect, and Lyα absorption by intervening systems is prevalent in spectra of especially distant quasars and galaxies (e.g. the Lyman α Forest, see Sect. 1.5). The importance of the Lyα transition in extragalactic astronomy can be gauged by the variety of fields in which it plays a pivot role, some of which will be described in more depth in this thesis. In the field of cosmology, Lyα can be used to probe the end of the Epoch of Reionization (EoR) (Dijkstra et al., 2007; Jensen et al., 2013; Malhotra and Rhoads, 2004), can be used to probe cosmic star formation rates and their variation with redshift (Ajiki et al., 2003; Hu et al., 1998; Kudritzki et al., 2000), to probe the cosmic Dark Matter large scale structure (Orsi et al., 2008; Ouchi et al., 2005, 2008; Venemans et al., 2002), and search for and map the earliest galaxies in the universe (e.g. Cowie and Hu, 1998; Giavalisco et al., 1996; Hartmann et al., 1984; Lacy et al., 1982), and more. However, the resonant nature of Lyα and the resulting radiative transfer effects can make it tricky to interpret observations correctly; both physical and spectroscopic morphology as well as luminosity is affected by this in ways that are not clearly understood, and thus inferring physical information from observations of these properties is not straightforward. This is the primary motivation for the work presented in Paper I and Paper II.

1.1 The Lyman α transition

Lyman α is the transition between the ground state and the first excited state in the neutral Hydrogen atom. The upper level is short lived, and the lower level is a singlet. This means that the ground state is richly populated and thus, photons of energy corresponding to the transition that encounter a neu-

tral hydrogen have a high probability of interaction. Since hydrogen, including atomic hydrogen, is very abundant in the Universe, that makes for a high absolute probability of interaction.

The Lyman α transition can be excited by either collision (which, when reemitted, is also known as *cooling radiation*) or by photon absorption. The latter case can again be subdivided into ionization and line absorption. Line absorption can only happen in certain narrow wavelength intervals between the Lyα wavelength of $\lambda = 1216$ Å and the *Lyman Limit* of 912 Å, the ionization wavelength of HI. Ionization, on the other hand, can happen at any wavelength shorter than the Lyman limit. Absorbed Lyα photons are almost immediately reemitted at the same wavelength and thus this absorption does not really contribute to the total amount of Lyα photons. 68% of recombination cascades will go through Lyα as the final step, as derived in Dijkstra (2014). Excitation through Lyβ to the second and higher excited levels can cascade down and result in the emission of a Lyα photon, but the contribution from this is small; the dominating contribution to total absorption-based Lyα production comes from recombination of ionized hydrogen. This contribution, in turn, dominates over the one stemming from cooling radiation (Dijkstra, 2014).

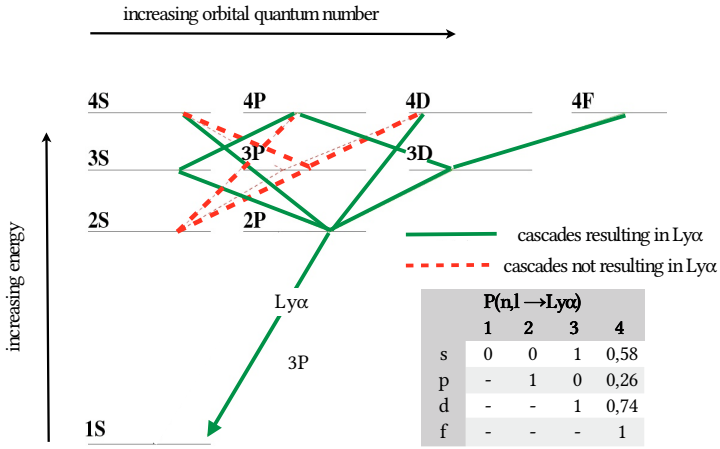

P(n,l →Lyα)	1	2	3	4
s	0	0	1	0,58
p	-	1	0	0,26
d	-	-	1	0,74
f	-	-	-	1

Figure 1.1: Diagram of transitions in the lowest levels of the neutral hydrogen atom. Green transitions can lead to an eventual Lyα emission, red transitions can not. The table on the lower left shows calculated probabilities that an electron in the given level/orbital combination will result in the emission of a Lyα photon. Figure from Dijkstra (2014), reproduced with permission.

In addition to the contributions mentioned above, a contribution also comes from blackbody radiation in stellar atmospheres, predominantly hot O and B stars. This contribution aligns with the general UV continuum in these stars

and does not produce any significant emission line effects, but will of course be subject to the same radiative transfer effects as the other contributions.

A simplified model of a galaxy spectrum resulting from the above mechanisms is shown in figure 1.2, taken from the important paper by Partridge and Peebles (1967) in which Lyα as a tool to find "primeval" galaxies was first suggested. Note that the spectrum is shown in frequency rather than wavelength space.

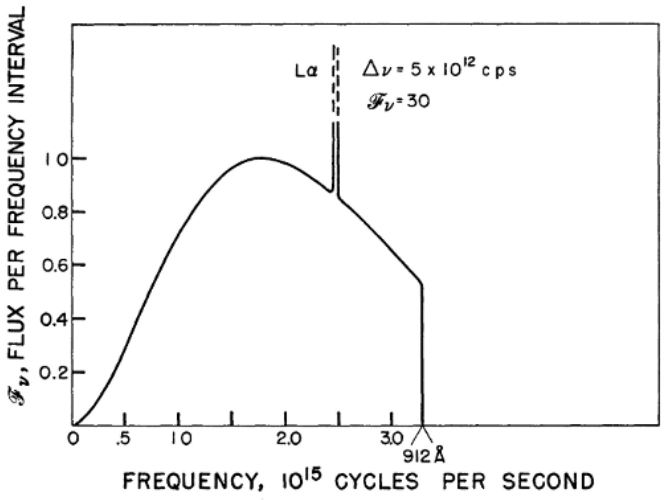

FIG. 3.—This curve represents semi-quantitatively the expected spectra of young galaxies in the extreme case that all photons of ionizing radiation have been converted to Lyman photons (§ IIe). The expected Lyman-α flux is calculated with $\Delta\nu = 0.002\ \nu$ for the line.

Figure 1.2: Figure from Partridge and Peebles (1967), showing a simple model of a blackbody spectrum after transmission through neutral hydrogen. © AAS, Reproduced with permission.

The figure shows a simple blackbody spectrum, from which all radiation blueward of the Lyman Limit is absorbed. Of this, approximately 1/3 of the flux is reprocessed into Lyα, illustrated as the narrow line, the strength of which is only hinted at in the figure, to keep the continuum clearly visible. The strength of the Lyα line, at first sight, promises a feature which should be visible either in spectroscopy or in narrow band imaging, at observed surface brightness levels where the continuum would be well below the noise level. With the then prevalent monolithic-collapse model of galaxy formation, which predicted galaxies to form at sizes comparable to that of the Milky Way, this would bode well for the feasibility of observing the first galaxies, even with the technology available at the time, assuming that the galaxies would have a redshift making Lyα fall within a redshift range in which IR airglow or absorption would not render these observations impossible. The authors themselves

assumed that galaxy formation and the resulting initial Lyα-brightness would fall within a cosmic "epoch of galaxy formation" at $z \sim 7$, in which case the first galaxies would not be observable from the ground, but noted that if this epoch was later, at e.g. $z \sim 4.5$, these galaxies should be readily observable from the ground.

While recombination is the dominating source of Lyα, collisionally excited cooling radiation can be significant especially in the outer regions of galaxies, far from star forming regions, where intergalactic cold gas is accreting onto the HI halo. When falling into the potential well of the galaxy, the potential energy is turned into kinetic and since heat energy, causing collisional excitation and ionisation of the H atoms, which will in turn cascade back while emitting Lyα and other lines as. Heat energy of the gas is emitted into radiation, cooling the gas (Dijkstra, 2014). It is not known exactly how and where cooling radiation is emitted. It has been proposed that it is mainly a shock process happening where the gas stream hits the galaxy, in which case the released gravitational energy could be substantial enough to be a significant contribution to some compact sources (Birnboim and Dekel, 2003; Dayal et al., 2010; Dijkstra and Loeb, 2009).

On the other hand, cooling radiation has also been proposed as a source of energy of the extremely extended Lyman α blobs (first observed by Steidel et al., 2000), in which case the shock should be weaker and the heating process less violent (e.g. Dijkstra and Loeb, 2009)

Hydrodynamic simulations have suggested that the fraction of Lyα contributed by cooling flows is rising with redshift, as the IGM is richer and accretion higher. The Lyα photon production is strongly temperature dependent, meaning that these results should be taken with caution. (Dayal et al., 2010)

In certain cases, galaxies are observed which have higher $W_{\mathrm{Ly}\alpha}$ than the $\sim 300 - 400$ Å which is the maximum for regular star formation (Laursen et al., 2013; Schaerer, 2003). In this case, a significant contribution could stem from cooling radiation, as this contributes only to the line strength and not to the underlying UV continuum (Kashikawa et al., 2012). However, the effect could also be due to Population III stars, as also suggested by these authors and others (Raiter et al., 2010; Schaerer, 2003), or star formation with a top/heavy IMF (Malhotra and Rhoads, 2002). Some of these effects can in principle be distinguished using Balmer lines, but these measurements would require an IR spectrograph with a sensitivity comparable to the next-generation James Webb Space Telescope which is currently under construction (Dijkstra, 2014).

1.2 Lyman α in emission

It was first suggested by Partridge and Peebles (1967) that the strength of the Lyman α transition could be used to detect primeval galaxies at high redshifts. Operating from the assumption that galaxies formed through Milky Way sized monolithic collapse, they predicted that it should be what later turned out to be unrealistically easy to detect these galaxies. They correctly assumed that young, star forming galaxies would have stronger star formation and thus higher surface brightness than typical spiral galaxies in the local Universe, but their estimate of the size of these protogalaxies was up to two orders of magnitude too large.

Theoretic models suggested that early galaxies, besides Lyα, should be strong emitters in UV continuum as well (Meier, 1976; Partridge and Peebles, 1967), but early observations yielded no detections.

No high redshift galaxies at all had been detected at the time, and no space-borne observatories had yet been launched to come clear of the atmosphere, impenetrable to UV; but it was believed that strong Lyα should in principle be detectable from such galaxies. However, when Meier and Terlevich (1981) used the International Ultraviolet Explorer to study local star forming galaxies, they found that only the most metal poor galaxy of their study showed any emission in Lyα. Later, also Charlot and Fall (1993) could show an, albeit weak, correlation, between metallicity and Lyman α.

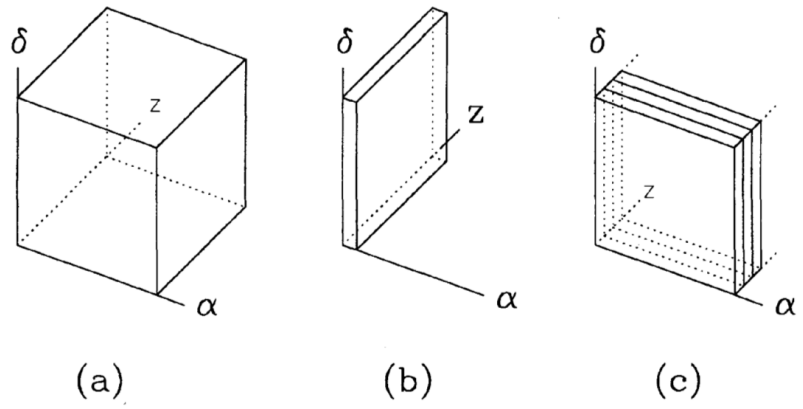

Figure 1.3: Sketch of different strategies for searching for distant galaxies. The strategies illustrated are, **left panel:** Slitless spectroscopy, **middle panel:** long-slit spectroscopy and **right panel:** narrowband surveys. Image from Pritchet (1994), reproduced with permission.

In figure 1.3 is sketched three important strategies when searching for strong emission lines in distant galaxies. They are:

Slitless spectroscopy This method is illustrated as a cube, because it both covers a large field of view (FOV) and a deep redshift range. This would at first glance seem like the ideal strategy for surveys. However, it has a quite severe shortcoming in that foreground from the entire image and at all wavelengths floods the detector and hence sets a limit to how deep such observations can go.

Long-slit spectroscopy This method only covers a small FOV, but a wide range of redshifts. It has the strong advantage over slitless spectroscopy that most atmospheric and Milky Way foreground radiation is blocked out by the slit, and the signal to noise (S/N) is dramatically improved. This allows for much deeper exposures and thus detection of fainter objects.

Multi-band photometry is depicted as a stack of flat layers, because it covers a large FOV (like slitless spectroscopy), but for each filter, it only covers a limited redshift range. Since light is not dispersed on a grating, foreground subtraction is much easier than for slitless spectroscopy. The method is based on the fact that an object with a strong emission line, when observed in a narrow bandpass centered somewhere close to the line center, will appear significantly brighter in these exposures than when viewed in broad filters, where the continuum dominates the integrated flux.

The latter method, then applied on optical and near-UV wavelengths, to which the atmosphere is still transparent, was first described in Haro (1956), in a form where three exposures through three filters were taken side-by-side on the same photographic plate. Certain galaxies showed extra strong blue/NUV emission in their central regions which were spectroscopically shown to also show strong emission in the O II λ3727 doublet as well as higher ionisation states, which he suggested could possibly make the method very useful in searching for galaxies with strong line emission.

In addition to these, a fourth method has gained strength since the publication of Pritchet (1994) in the shape of Integral Field Spectroscopy. IFS combines the advantages of long-slit spectroscopy - wide redshift coverage, low foreground allowing deep exposures - with the advantages of the wider FOV coverage and the spatial resolution in multi-band photometry. IFUs can be used to probe the Ly-α luminosity function in a deeper volume than that of narrow-band imaging, spatially resolved and with a much larger FOV than that of a classic spectrograph, as done by e.g. van Breukelen et al. (2005). Integral field spectroscopy can also directly spatially map continuum subtracted Ly-α (at redshifts allowing transmission through the Earth's atmosphere) with significantly less model dependence, like e.g. done with the MUSE IFU by

Wisotzki et al. (2016). IFUs like MUSE, which can compete simultaneously with the spatial resolution of imaging cameras and the spectral resolution and wavelength coverage of typical spectrographs are still very expensive and the time allocation highly competitive.

1.2.1 Early attempts at observing the first galaxies in Lyα

Already from the earliest theoretical studies of the first, "primeval" galaxies, it was suggested that studying strong star forming regions in the local and nearby Universe in the UV could provide hints of what young galaxies in earlier epochs would look like and thus what to look for (Meier, 1976; Meier and Terlevich, 1981; Partridge and Peebles, 1967). It was predicted that Lyman α would be strong, but had already been observed to not follow theoretical predictions in observations of quasars.

However, it was only with the launch of the International Ultraviolet Explorer (IUE) in 1978 that the UV Universe became possible to observe. Meier and Terlevich (1981) were the first to observe in UV the hot HII regions surrounding regions of strong star formation in nearby galaxies. Their study targeted three galaxies close enough to be viably observed while still with enough redshift to shift Lyα out of the strong geocoronal line. Based on the strength of the Balmer lines in these galaxies, Lyα was expected to have a strength in emission comparable to that of the geocoronal feature. What they found was that only one of the three objects showed any emission at all, and that at only 1/6 of the strength expected from recombination theory. The researchers conclude that the most likely reason for the deficit in Lyα emission is dust, but note that the Balmer deficit does not seem to be consistent with the amounts of dust necessary to absorb these amounts of Lyα.

Similar results were reached by Lacy et al. (1982), who had used the IUE to observe a sample of Seyfert galaxies. Lyα luminosity was consistently lower than predicted from recombination theory. The authors conclude that simple dust reddening as an explanation of this is not consistent with observed line ratios in Hα, Hβ and Pα. Instead, they suggest that a combination of dust, collisional deexcitation in high density regions and the higher optical depth traversed by a Lyα photon due to resonant scattering could join forces to bring down Lyα luminosity. It seemed apparent already at this point that ISM transmissivity of Lyα in HI regions is a complicated, multi-parameter problem.

Hartmann et al. (1984) show reach similar results in the paper named "How to find galaxies at high redshift". Measuring the spectra of three nearby galaxies, they measure only weak Lyα in two of them and none in the third and conclude that Lyα might not be as easy to observe as was predicted by Partridge and Peebles (1967). They suggest that the suppression of Lyα could be

due to a combination of dust and the longer optical path of Lyα in HI systems resulting from resonant scattering.

Giavalisco et al. (1996) performed a re-analysis of the IUE archival data (Hayes, 2015), using a more mature reduction pipeline and spatially matched the IUE aperture with those used for obtaining optical line spectroscopy. They found that dust reddening and oxygen abundances had insignificant and only weak influence on Lyα equivalent width; suggesting that the optical path length was more important than actual dust content (measured by Balmer decrement) or metallicity. This stood in contradiction to the conclusions by Charlot and Fall (1993), who, found a correlation between $W_{\mathrm{Ly}\alpha}$ and metallicity. Interpreting metallicity as a proxy of dust content, and comparing to models of Lyα escape at various conditions, they claim that Lyα can only escape in significant fractions if a galaxy is dust-free, or an AGN is present, and suggest that this would make Lyα emission useless as a beacon of primeval galaxies, instead of which they propose Hα, despite its lower intrinsic brightness, might be a more suitable target, because it can escape freely.

1.2.2 Size and luminosity of early galaxies

One important assumption that made the predictions of Partridge and Peebles (1967) unrealistically optimistic was the then prevalent model of galaxy formation by monolithic collapse. The model predicted that galaxies would form to have sizes comparable to that of the Milky Way. Given a certain star formation rate per mass unit (SFR), this would on one hand predict much more luminous galaxies than the ones currently observed at high redshift; on the other hand, it would spread out the O star luminosity over a larger area and thus give a reduced surface brightness. It was expected that a galaxy formed through monolithic collapse would have the majority of its star formation going on in a relatively dense central region, raising the surface brightness above what would be expected if it were equally distributed throughout the galaxy.

Simulations and theoretical considerations of Baron and White (1987) predict that galaxies, rather than monolithic collapse, assemble hierarchically and that strong star formation episodes set in in knots and generally have a life time comparable to the free fall collapse time of these knots into a galaxy. They predict that not only should star forming knots be smaller than the earlier predicted central regions of large spirals; the galaxies would generally be fainter than earlier predictions.

Pritchet (1994) argues that the collapse time of a galaxy of Milky Way type is such that, given that cosmological parameters at the time were considerably more poorly constrained than at present, this type of galaxy could at the earliest be formed at a redshift between $z = 1.8$ and $z = 3.5$. This is of course a rather

poor constraint, but it does predict that any galaxies formed at redshifts higher than this would have to be considerably smaller than this size. Pritchet (1994) continues to sum up a number of surveys for Lyα emitting galaxies carried out with the IUE in order to constrain at which redshifts galaxy formation has happened, as well as typical sizes and morphologies of these primeval galaxies. These surveys are compared to the simple galaxy formation models of Baron and White (1987), building on monolithic collapse with some room for clumpiness. The authors conclude that at the time of writing, the surveys carried out so far should have led to the observation of 10^{1-3} primeval galaxies in Lyα. However, not one convincing candidate had yet been found.

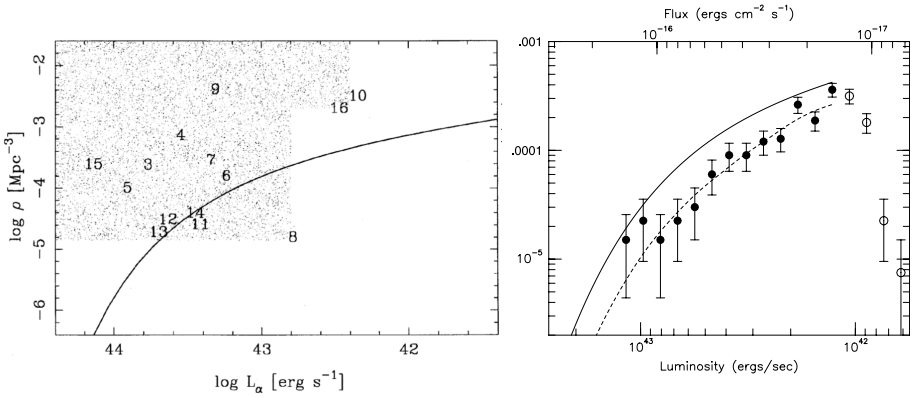

Figure 1.4: Left panel: Model luminosity function from Baron and White (1987), shown in figure from Pritchet (1994). Shaded areas are values of luminosity and number density which had been probed by surveys at the time with no PG candidates detected so far. Numbers are references to works in which the limits, represented by their placements, were reached. **Right panel:** Empirical luminosity function found by Gronwall et al. (2007) for galaxies at redshifts ~ 3 in the Extended Chandra Deep Field South through the MUSYC survey. Right panel © AAS. Reproduced with permission.

Figure 1.4 shows in the left panel the luminosities and number densities probed by the surveys reviewed in Pritchet (1994), along with the model luminosity function of Baron and White (1987). No primeval galaxy candidates are found in the area surveyed, constraining the possible real luminosity function to the white area in the lower right of the panel. In the right panel is shown the empirical luminosity function found by Gronwall et al. (2007) for galaxies at $z \approx 3$ from the MUSYC survey in the Extended Chandra Deep Field South. The axis scale is slightly off, but by comparing the axes it can be seen that Gronwall's luminosity function actually does fit in the white lower right area, although it may overlap slightly with the shaded area around the number 8 in the left frame.

The luminosity function of Gronwall et al. (2007) is roughly an order of magnitude lower than the one from Baron and White (1987). This was already hinted at in Pritchet (1994). The authors suggest two mechanisms which could possibly explain this discrepancy. One is dust content: a weak correlation had been found the year before by Charlot and Fall (1993) (see above for discussion of this). However, the constraints in figure 1.4 have already been corrected for dust extinction, and yet there is a large discrepancy unaccounted for.

The second mechanism discussed by the authors is that angular extent could lead to lower surface density given constant total luminosity, which with the then current quantum efficiency of detectors could lead to a degradation of surface density rendering the galaxy undetectable. However, such an effect, even at its strongest, could only account for a fraction of the discrepancy.

What they do not discuss is the assumed size of the primeval galaxies. Pritchet (1994) adopt an angular size of ≈ 5", corresponding (in the then-favored cosmology) to a physical size of 30-40 kpc for $z = 2 - 5$ for the new formed galaxies, while later surveys have shown a physical extent an order of magnitude lower. As an example, Bond et al. (2009) find typical sizes of to be ≈ 2 kpc at $z = 2$. Besides yielding a much lower total luminosity than expected with the monolithic-collapse models, this also means that galaxies at these distances are unresolved or close to the resolution limit even with current technology, while Pritchet expected them to be resolved even with contemporary technology. Expressed in angular size, Malhotra et al. (2012) report almost constant LAE (see sect. 1.2.4) sizes of ~ 1.5" over a redshift range of $z = 2 - 6$, while Ferguson et al. (2004) report angular sizes of LBGs (see sect. 1.2.3) to vary between 1.2 and 4.8" at redshifts between 2 and 6.

1.2.3 Lyman Break Galaxies

The Lyman Break technique does not rely directly on Lyα; but it is an important method to survey and select high redshift galaxies of a type which could potentially have strong intrinsic Lyα luminosity. Lyman Break selection is a method to select galaxies at a given redshift based on the spectral luminosity dropout that happens at the Lyman Limit, as shown in e.g. fig. 1.2. The method is first described by Steidel et al. (1996)). It relies on obtaining imaging through multiple broad-band filters (Steidel and Hamilton, 1993). Blueward of the redshifted wavelength of the rest-frame Lyman Limit (912 Å), the observed flux will drop drastically, often disappear entirely, compare to the redder bands. This drop-out provides a coarse approximation to the redshift of the object, although follow-up spectroscopy is needed to confirm the redshift and assert it with higher precision. The method relies on a relatively strong continuum in the blue and UV and thus a strong and relatively young stellar

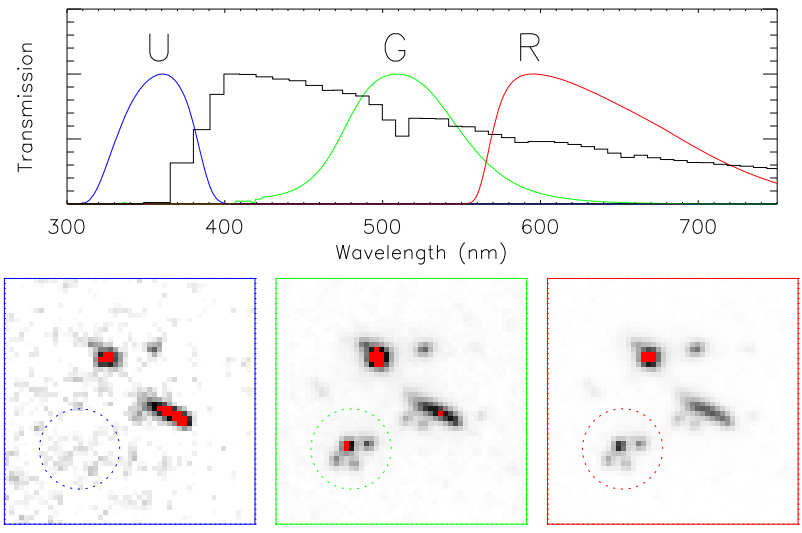

Figure 1.5: The Lyman break method illustrated. The upper panel shows a typical galaxy spectrum, with the sensitivity curves of the three filters overlaid in blue, green, red. Lower panels show images of the same field in these three filters. One galaxy, encircled, is visible in the G and R filters, but invisible in the B filter. Image kindly provided by Johan Fynbo, DARK Cosmology Centre.

population. Secondly, it relies on the ISM/CGM of the galaxies in question to be opaque to ionizing radiation. The latter is not a strong requirement; at redshifts where this technique is typically applied, the IGM effectively suppresses all Lyman Continuum radiation.

The method is illustrated in figure 1.5, the upper panel of which shows a low-resolution spectrum of a star forming galaxy with strong stellar continuum radiation in the rest frame blue and UV. Overlaid is the sensitivity curves of the three filters used to detect the drop-out. The lower panels show images of the same field observed with the corresponding filters. One galaxy, encircled, is clearly visible in the G and R filters, but is not detected in the U filter, meaning its Lyman Break is situated at a wavelength somewhere between the U and G filters' ranges of sensitivity. The illustration also shows very well how coarse grained redshift estimation is with this method; from the upper panel it is clear that the galaxy could be redshifted by another 50-75 nm and still not look very different in the images. It is clear that spectroscopic follow-up is necessary in order to confirm the redshifts of candidate objects detected in this way. On the positive side, the use of broad band filters only allows for better throughput and deeper searches.

In the original paper (Steidel et al., 1996), the filters are chosen to select

objects with redshifts between approximately 3 and 3.5, where the bluest filter is falling on the blue side of the observed Lyman Limit, and the Lyα forest (see Sect. 1.5) is not strong enough to reduce the flux in the band covering the wavelengths between Lyα and the Lyman Limit so much that it could cause a drop-out or ambiguity in said filter. The first fields searched were in the vicinity of known QSOs with absorbing Lyman Limit systems (see Sect. 1.5) at redshifts $z \gtrsim 3$, since galaxies tend to clump together and thus one is more likely to find galaxies in the vicinity of other galaxies. The method was immediately successful in detecting a substantial population of galaxies at these, at the time, extreme redshifts.

Since then, with the advent of better IR detectors, the redshift limit for detections has been continuously pushed (i.e. Bouwens et al., 2007, 2008; Ly et al., 2009, 2011; Madau et al., 1996; Pentericci et al., 2010; Shapley et al., 2003; Steidel et al., 1999, 2003) till today, galaxies up to redshifts of $z = 11$ have been detected (Oesch et al., 2013).

1.2.4 Lyman Alpha Emitting galaxies (LAEs)

Due to the tentative anticorrelation between metallicity and W(Lyα) found by Meier and Terlevich (1981) (which was later confirmed by study of two extremely metal-poor galaxies by Terlevich et al. (1993)), they noted that it was unfortunate that the galaxy with lowest known metallicity, I Zwicky 18 (I Zw 18), had a too small redshift to be observed with the IUE, since it was expected to show very strong Lyα luminosity.

In 1990, the Hubble Space Telescope was launched, and on board among the first generation of instruments was the *Goddard High Resolution Spectrograph* (GHRS), which had a higher resolution power than the IUE by a factor of 10-100 (Hayes, 2015). With this improved resolution, it became possible to come closer in redshift while still keeping the target Lyα feature free of geocoronal Lyα. With the GHRS, I Zw 18 was observed by Kunth et al. (1994) who surprisingly found, not strong emission, but a deep Lyα absorption feature with broad damping wings. This was puzzling, as it was a strong deviation from the W(Lyα)-metallicity anticorrelation expected, and posed a strong contradiction to the dust dependence of Lyα escape claimed by Charlot and Fall (1993). The authors conclude that even very low dust content can suppress Lyα escape through the longer optical path traveled by the photon. Adding to this effect, they note that if Lyα is resonantly scattered in large HI systems surrounding the emitting HII regions, and this extended HI system is then mostly covered by a narrow slit, then most of the reemitted photons will be blocked out with it.

Lequeux et al. (1995) perform similar observations of the galaxy Haro 2;

a comparison of the Lyα spectral features of I Zw 18 and Haro 2 can be seen in Hayes (2015), fig. 3. Despite having a much higher dust content than I Zw 18, it shows strong emission in Lyα. The line shows a clear P Cygni-type line shape, suggesting that the light has been scattered in an outflowing medium. This further weakens the case for the claims of Charlot and Fall (1993), and suggests that an outflowing medium may provide a way for Lyα to escape even through a dust-rich HI medium.

This line of thought is pursued further in Kunth et al. (1998), in which the authors undertake the study of hot HII regions in 8 nearby galaxies. The authors find that only 4 of these galaxies show Lyα emission, and all of these have P Cygni type emission lines, with a redshifted main emission feature and a blueshifted emission trough, again the tell-tale sign of scattering in an expanding medium, further strengthening the idea that gas kinematics, rather than neutral gas or dust content, is the most important. Although later studies have suggested that no single mechanism determines Lyα escape and line shape, the importance of outflows have since been confirmed in e.g. Wofford et al. (2013), Jones et al. (2013), and in Paper II.

1.2.5 Lyman α emission at high redshift

A breakthrough in the hunt for primeval galaxies came with Hu et al. (1998) and Cowie and Hu (1998), who reported the detection of a sample of 15 Lyman α emitting galaxies at redshifts 3-6 using narrowband search of blank fields on the then new 10 meter Keck telescope. This was the first of the 10-meter class telescopes which, with their larger light gathering area and new detectors with improved quantum efficiency, were the first to provide the sensitivity necessary to detect high-redshift star forming galaxies in larger numbers. Since then, extensive studies have been carried out targeting both LBGs and LAEs at high redshifts. The record is often moved further away; at the time of writing, the farthest object observed is a spectroscopically confirmed LBG at redshift $z = 11$ announced by Oesch et al. (2016), and the physical properties and their evolution of Lyman α emitting galaxies at redshifts out to $z \sim 7$ have been studied in depth with regards to age, stellar mass, dust content, star formation rates, clustering etc.

LBGs and LAEs are drawn from the same population, but based on different criteria with different bias: LBGs are biased towards a strong UV luminosity and thus a strong stellar population, whereas LAEs are selected with a bias for specific star formation rate, which tends to favor younger, low-mass galaxies, because a significant existing stellar population will create a stronger UV continuum and thus lower W(Lyα). Shapley et al. (2003) studied a large sample of spectra of LBGs at redshift $z \sim 3$ and found that $\sim 25\%$ of the sample

had rest-frame W(Lyα) > 20 Å, the usual criterion for LAE selection. Shapley et al. (2003) also found that LAEs in their sample showed a bluer UV continuum than the non-emitters, reflecting a younger stellar population (probably a product of ongoing or recent episodes of strong star formation). This has later been confirmed at different redshifts by e.g. Cowie et al. (2010, 2011).

Earlier studies have shown that LAEs are small (Dijkstra et al., 2006), low-mass objects (e.g. Finkelstein et al., 2007; Gawiser et al., 2006); however, the trend does not always hold. Pentericci et al. (2009) report masses up to $5 \times 10^{10} M_{\odot}$, and Hagen et al. (2014) report that their sample of LAEs from the HETDEX pilot study shows masses representative of the expected general mass function for star-forming galaxies. LAEs are likely to be in their early stages of starbursts (Gawiser et al., 2006, 2007) or immediately post-burst (Hayes, 2015), although some can have a significant age and underlying stellar population (Pentericci et al., 2009), implying that if these are undergoing a star formation episode, it is not necessarily the first. These older galaxies from Pentericci et al. (2009) were LBGs selected to also be LAEs. There is however a trend for the strongest LAEs to all be very young, small, dust-free objects (Finkelstein et al., 2007; Pirzkal et al., 2007; Venemans et al., 2005).

Morphologically, LAEs tend to be compact (Gronwall et al., 2007; Malhotra et al., 2012; Pirzkal et al., 2007); Bond et al. (2009) reports half-light radii of $\lesssim 2$ kpc and a typical value of ≈ 1.5 kpc at $z = 3$, while they cite LBG studies at comparable redshifts with typical extend of ≈ 2.27 kpc. LAEs are compact, irregular/merging systems and face-on spirals (Cowie et al., 2010; Venemans et al., 2005; Verhamme et al., 2012). Malhotra et al. (2012) show that LAEs have a typical, constant size over a redshift range $2.25 \lesssim z \lesssim 7$ and conclude that small size is an important factor determining whether a galaxy will show Lyα emission. The Lyα luminosity function (LF) of LAEs is largely unchanged at redshifts 2 - 6, while the UV LF evolves strongly within same redshift interval (Ouchi et al., 2008). Between $z = 5.7$ and $z = 6.6$, however, the LF of Lyα decreases by 30% (Ouchi et al., 2010) – see Sect. 1.6.3 for more about this. Lyα escape fraction rises strongly between redshifts $z = 0.3 - 6$, from $\lesssim 1\%$ to $\approx 40\%$, following a power law and predicting $f_{\rm esc}$ to become unity at $z \approx 11$ (Hayes et al., 2011). However, at $z \gtrsim 6$, the distribution dips somewhat, a change that is likely due to either a growing neutral fraction of the IGM, an increase in ionizing photon escape, or a combination hereof.

1.3 Pilot study: Lyman α Morphology in nearby galaxies

Surveys of LAEs at high redshifts described above rely heavily on Lyα as a bright line visible well above the limiting fluxes of the continuum. However, as we have also seen, the Lyα escape fraction is strongly dependent on a num-

ber of factors counting among the most important HI optical depth, galactic wind outflow velocities, dust content and ISM geometry. When not completely absorbed, Lyα can scatter numerous times in the neutral medium before escaping, after which we would predict the galaxy's morphology in Lyα to be strongly affected by this. Some early studies (e.g. Fynbo et al., 2001; Moller and Warren, 1998) have shown that some high redshift sources do indeed seem smeared in Lyα although they appear almost point source-like in continuum.

Even if the entire intrinsic Lyα flux would escape the galaxy, it would, as predicted by e.g. Laursen et al. (2009a), be with a significantly lower surface density, which could furthermore be anisotropic and therefore appear even fainter. This larger extent could bring systems at high z, which would otherwise be detectable, below the limiting Lyα flux of a given survey. Adding to this, there is the problem of dust absorbing Lyα photons and thus introducing another source of uncertainty to high redshift surveys.

To correctly interpret the observations done at high redshifts, it is of great importance to gain some understanding of which physical factors govern Lyα radiative transfer. However, practically all observation campaigns in Lyα of nearby galaxies had until a decade ago been in spectroscopy; almost nothing was known about the morphological properties in Lyα in these galaxies compared to those in UV/optical continuum.

At low redshifts, the galaxies observed have such large extents that the spectrometer aperture often only covers a small fraction of the entire galaxy. While this is fine for investigating local properties around the central star forming regions, it does pose a problem for Lyα. Due to the resonant scattering, Lyα escape, in fact any property in Lyα, should be viewed as a global rather than local property. Lyα escape fractions simply cannot reliably be measured inside a spectrometer aperture, because a substantial fraction of the radiation, even if it is all produced in a region entirely contained within the aperture, might scatter in the neutral medium and be transported far outside the aperture before escaping the galaxy. In principle, a galaxy might be a deep, damped absorber inside the aperture while still globally be emitting more strongly in Lyα that can be accounted for by stellar continuum.

To remedy this, the first attempts at observing the morphology of continuum-subtracted were done in 2005 (Hayes et al., 2005). The strongly star forming Blue Compact Galaxy ESO-338 IG04 (aka. Tololo 1924-416) was observed in a narrow band around its redshifted Lyman α and in continuum with the Solar Bind Channel (SBC) of the Advanced Camera for Surveys (ACS) at the Hubble Space Telescope (HST) (Hayes et al., 2005). An important part of the project was to develop a reliable way to subtract continuum. For this to be done, it is necessary to create detailed models of the underlying stellar population and subtract the modelled continuum in side the narrow band from the

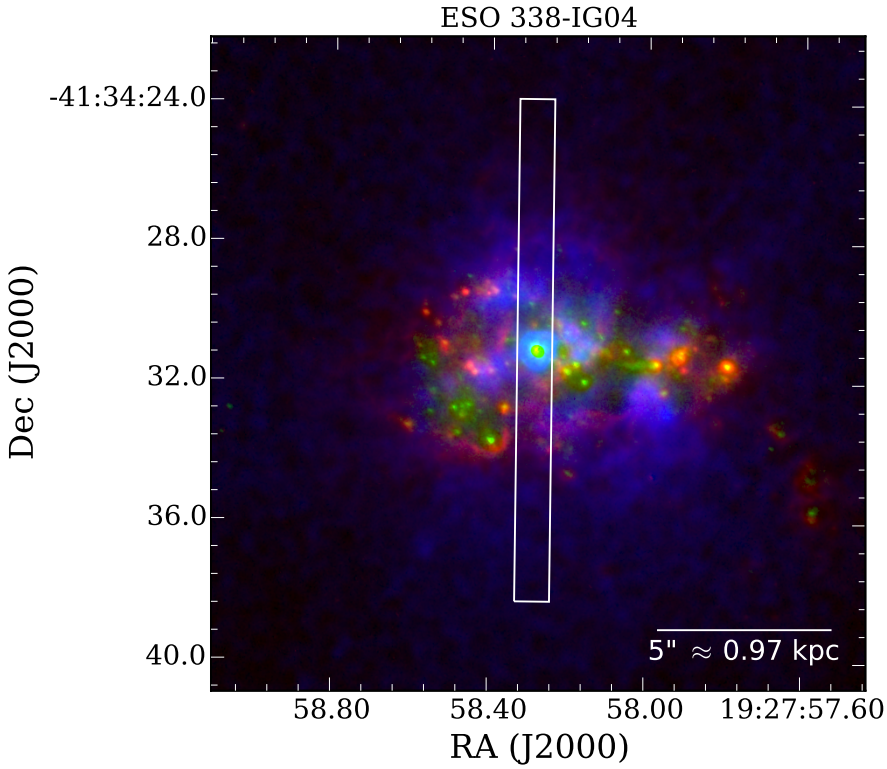

Figure 1.6: RGB image of ESO 338-IG04 in UV Continuum (green), Hα (red) and Lyα (blue). Overlaid is the approximate position of the synthesized slit used in Paper III. The figure is made from data presented in Hayes et al. (2009), Östlin et al. (2009).

observed flux.

This method was further developed and implemented on a small sample of 6 galaxies a few years later (Hayes et al., 2009, Östlin et al. (2009)), in which the continuum modelling procedure was considerably refined. These galaxies all showed a wide range of Lyα emissivity, from large halos to practically no emission at all.

Figure 1.6 shows a false color image of ESO-338 IG04 created from the data output from Hayes et al. (2009). Green shows UV continuum, tracing the hot OB star forming knots in the galaxy. Red is Hα, which traces the hot HII regions in which recombination takes place; this also traces intrinsic Lyα production in a fixed rate with Hα. Blue shows continuum-subtracted Lyα. The extended radiation of Lyα shows little resemblance to the configuration of HII regions; the central star forming know is bright in all three bands, but

apart from this, Lyα appears to shine smoothly from a large, extended halo surrounding the central luminous regions. Lyman α morphology does indeed seem to be largely decoupled from that of the continuum; a large fraction of emitted Lyα is indeed transported to and emitted at distances far from the HII regions of their origin. It would be clear that a survey like this should be of interest as grounds for comparison to high-z samples. However, six galaxies do not constitute a representative sample, and the group suffers from certain selection biases. But this pilot study provided an important proof of concept and a strong argument for investing more telescope time in pursuit of a statistically useful sample of star-forming, Lyα producing galaxies.

1.4 Lyman α radiative transfer in galaxies

An atomic transition being resonantly scattered in a medium as abundant as HI is bound to have profound effects on radiation stemming from this transition, and investigating the effects of this scattering on an intrinsic line passing through the ISM in a galaxy before escaping has been the subject of a large body of theoretical as well as observational research, some of which has already been mentioned above.

1.4.1 Dust

When the first searches for primeval galaxies as mentioned in Chapter 1.2.1 yielded no detections; one of the main explanations suggested was dust attenuation (Hartmann et al., 1984; Meier and Terlevich, 1981). It had been known at least since Osterbrock (1962) that a Lyα photon undergoes a much larger number of scatterings before escaping the galaxy than does a photon from the nearby continuum. This would mean a larger probability of being absorbed by dust due to the longer path the photon would travel through the medium before escaping. Early reports suggested that dust content might thus be the main factor determining Lyα escape. However, Neufeld (1990) showed that due to the very long optical paths travelled by Lyα photons in a HI medium, even minuscule amounts of dust could almost completely eradicate Lyα photons from an emitted spectrum. This would suggest that the length of the path travelled, and hence the column density N_{HI} was of comparable importance as dust content. The correlation between dust and Lyα luminosity found by the earliest searches was only weak and tentative, and while Charlot and Fall (1993) claimed to find a clearer correlation, the reanalysis of earlier data by Giavalisco et al. (1996) showed no significant correlation. Later searches have shown that there is a correlation between dust and Lyα escape, albeit with a

large scatter, suggesting that the relation is not a simple one (see e.g. Atek et al., 2014)

Not only dust content, but also the geometry of dust and HI plays a role. Neufeld (1991) concluded that while a uniform, static medium was almost certain to produce deep Lyα absorption, a two-phase medium of dense, dusty clumps embedded in an attenuated, dust-free gas could let some Lyα escape and could even in certain circumstances enhance W(Lyα) beyond its intrinsic level. Scarlata et al. (2009) show that as long as the dust is distributed in clumps, the gas density of the surrounding medium is less important; while a uniform dust screen is inconsistent with observations, these can be reproduced by assuming a clumpy dust screen, in which it is not required for Lyα to bounce off the surface of these clumps as suggested in the Neufeld model. Furthermore, Laursen et al. (2013) and Duval et al. (2014) show by numerical simulations that the Neufeld scenario only works in very special and unrealistic conditions and produces emerging spectra that are inconsistent with most observed spectra with enhanced W(Lyα).

1.4.2 HI mass

As the observations of I Zw 18 by Kunth et al. (1994) show, dust content alone can not be the only, and probably not even the main, determining factor of Lyα escape. I Zw 18 is a damped Lyman α absorber, despite having one of the lowest oxygen abundances of any known galaxy. The number of dust grains encountered while traversing the system is determined not only, and perhaps not even mainly, by the number of dust grains present; but may rely more sensitively on the length of the optical path, which is again depends strongly on raw number of HI atoms present. I Zw 18 has a very high HI mass compared to its stellar mass which can explain the strong absorption despite the low metallicity.

Even in the absence of dust, a high HI mass can have a strong impact on the shape of the spectral line of Lyα, as shown by Neufeld (1990), who did an analytic model of resonant scattering in a static HI medium. Due to line broadening (thermal or natural, see Sect. 1.5), each scattering event will red- or blueshift a photon by an amount drawn from the line profile distribution. The more strongly a photon is shifted, the lower its probability of interaction with any subsequent atom it encounters and thus the higher its escape probability. As a result, an emerging line profile from Neufelds static, dust-free medium will consist of a strong absorption feature at line center and the intrinsic flux equally distributed in a red- and a blueshifted emission component. The width and strength of this composite line depends strongly on HI mass; higher mass will suppress emission at a wider range of wavelengths and lead

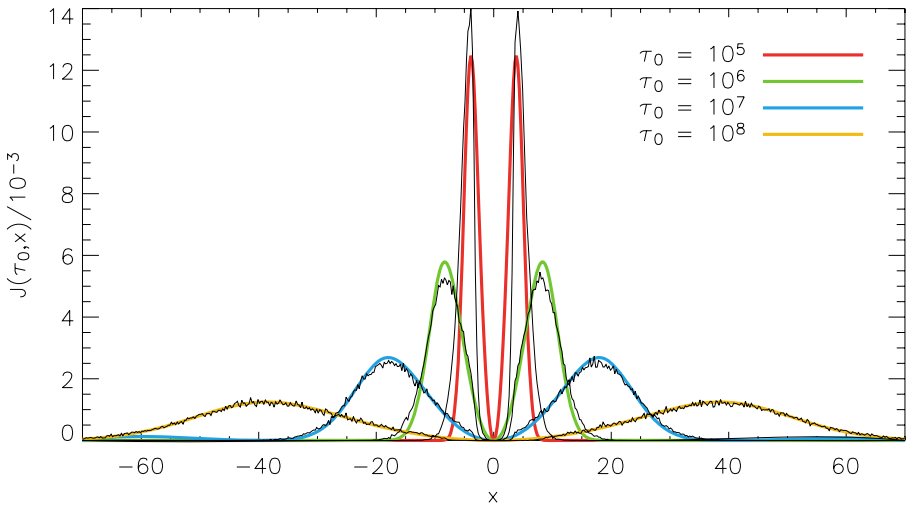

Figure 1.7: The effect of Lyα optical depth of a line profile emerging from a static, dust/free medium. Colored profiles are analytic solutions from Neufeld (1990), black lines are simulated spectra from Laursen et al. (2009a). The figure is from the same paper, © AAS, reproduced with permission.

to a broad doublet with relatively low peak, while lower HI mass will mean a lower intrinsic interaction probability and thus a narrower, taller double-peak profile. Actual double-peaked profiles are rare to observe and are exclusively observed in systems at low column density (e.g. Jaskot and Oey, 2014). Pardy et al. (2014) report that higher HI mass does indeed suppress both W(Lyα), $f_{\rm esc}^{\rm Ly\alpha}$ and Lyα luminosity for a sample of 12 nearby, star-forming galaxies (see Sect. 3).

1.4.3 HI kinematics & Geometry

While the observation of I Zw 18 suggested HI mass to be a governing factor of Lyα escape, the subsequent observation of a strong P Cygni Lyα profile in Haro 2 (Lequeux et al., 1995, see Sect. 1.2.4) and the observations of Kunth et al. (1998) linking outflows to Lyα escape and consistently showing blueshifted UV metal absorption lines indicates that also HI kinematics is important for the escape of Lyα radiation. The idea is elaborated further by e.g. Mas-Hesse et al. (2003), who interprets different Lyα spectral profiles as steps in an evolutionary sequence in which star formation feedback transforms an initially thick and static halo into an expanding, thin superbubble build on the model by Tenorio-Tagle et al. (1999); each step in the evolution showing different spectroscopic fingerprints in Lyα.

The effects of kinematics and geometry have been investigated theoreti-

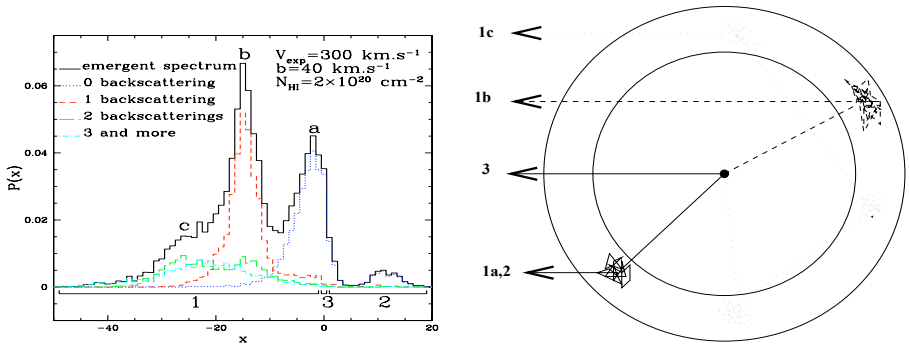

Figure 1.8: Left panel:: emerging line profile of Lyα from an expanding HI shell model shown in black, along with the single component. **Right panel:** Sketch of expanding shell model with sketch of different paths travelled by Lyα photons. The numbers 1a-c, 2, 3 correspond to components in the left panel. Image from Verhamme et al. (2006), page 407, reproduced with permission from the author and the journal, © ESO.

cally in great depth for decades, from general models of resonant scattering in an optically thick medium (e.g. Adams, 1972; Neufeld, 1990, 1991; Osterbrock, 1962), to more realistic models of star forming galaxies (e.g. Duval et al., 2014; Hansen and Oh, 2006; Laursen and Sommer-Larsen, 2007; Laursen et al., 2009a, 2013; Verhamme et al., 2006, 2008).

In figure 1.8 is shown a schematic of the effects of Lyα radiative transfer on the spectrum emerging from an expanding shell of HI. In the left panel is shown in black the resulting line profile, in colors are shown individual spectral contributions resulting from different paths travelled by the photons. These paths are sketched in the right panel, which shows the central monochromatic source, the expanding shell and four different paths each yielding different spectroscopic characteristics. The numbers 1a-c, 2, 3 correspond to component numbering in the left panel. Components 1a and 2 are shown in blue, and consist of photons that are emitted at line center in the center of the system. When reaching the expanding shell, they diffuse through it, after which a fraction of them will escape as a double-peaked profile as described in Neufeld (1990), except the photons are redshifted somewhat relative to the rest frame of the expanding medium, the line profile of which will therefore be stronger on the blue side of the line than on the red, introducing the asymmetry that is seen in the figure.

Component 1b, shown in the left panel in red, consists of photons that have originally been emitted towards the receding far side of the expanding shell, from which it has been backscattered and emitted towards the viewer (on the left, at infinite distance). This backscattering happens at a wavelength

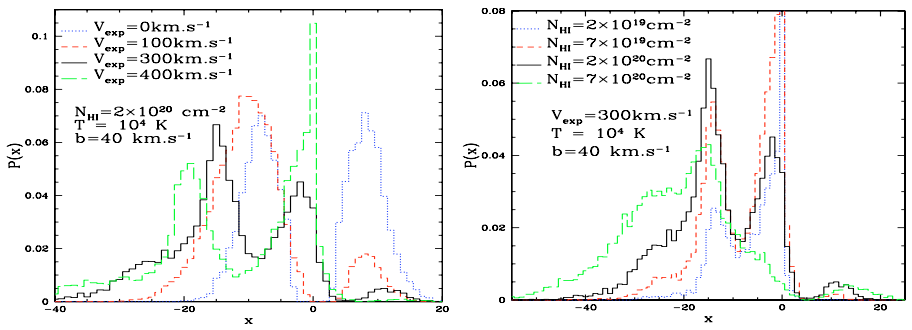

Figure 1.9: Left panel: The effect of outflow velocity on the components of Fig. 1.8. **Right panel:** The effect of HI column density on the components of fig. 1.8. Image credit: Verhamme et al. (2006), pages 408 and 409, reproduced with permission from the author and the journal, © ESO.

distribution centered around rest frame Lyα line center, resulting in a peak redshifted by twice the velocity of the outflowing medium. This component is predicted to be *stronger* that peak 1a, because it is strongly redshifted wrt. the approaching front side of the shell and thus has a much higher escape probability. Component 1c is weak and diffuse and represents photons that have undergone two or more backscatterings.

Finally, component 3 represents direct escape. At strong outflow velocities and/or low column densities (or, not treated here, in configurations with a perforated neutral medium), a fraction of the emitted photons will escape directly, with no interactions and thus not affected by any radiative transfer effects.

Inhomogeneous, multiphase HI systems can, even in the absence of any dust, show anisotropic Lyα escape and thus the surface brightness and derived luminosity of a test galaxy could vary by an order of magnitude and a factor of ~ 4, respectively (Laursen and Sommer-Larsen, 2007, Laursen et al. (2009b)); the presence of dust can affect the overall escape fraction but does not change the angle dependency of surface brightness, and the derived luminosity can vary with a factor of $\sim 3-6$ based on angle (Laursen et al., 2009a). Geometric effects have also been modelled by Verhamme et al. (2012), who show that the orientation of a disk galaxy is important, Lyα escape is more likely in face-on than edge-on spirals. This is in agreement with e.g. observations by Cowie et al. (2010). Not only L(Lyα) but also W(Lyα) can be affected strongly by viewing angle (Gronke and Dijkstra, 2014).

Rearranging a homogeneous medium into denser clumps and a sparser interclump medium will allow a larger fraction of Lyα to escape, but will not affect its spectral line shape; i.e. it affects all components equally (Duval et al., 2014; Laursen et al., 2013). A very thin interclump medium will allow for di-

rect escape even at line center the same way it will happen in a very optically thin homogeneous medium.

1.5 Lyman α absorption systems

Also en route between the emitting system and the telescope can the Lyα transition have an interesting impact on the light. As light from a distant source traverses the Universe, it gets continually redshifted. Whenever it encounters an HI system, this leaves an absorption feature in the spectrum at the Lyα rest/frame wavelength of the given system. The depth and width of this feature depends on the column density of the system, i.e. how many atoms in total will be contained within a cylinder of base area 1 cm^2 around the sight line to the emitting system. The systems are grouped into three different kinds based on their observed column densities: system with column densities $N < 10^{17} \cdot \mathrm{cm}^{-1}$ generally show saturated but narrow, Gaussian-like absorption features. These systems are present in high numbers in the high redshift Universe and leave a characteristic pattern of narrow, dense absorption lines blueward of rest-frame Lyα of a background emitting galaxy.

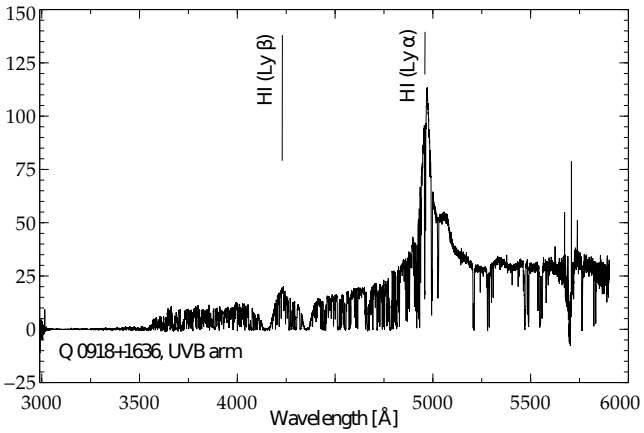

Figure 1.10: Example of Lyman α forest seen blueward of the Lyman α emission line of the quasar Q0918+1636. Two DLA systems are also present, one on each side of the Lyman β emission line of the quasar.

This pattern is widely called the *Lyman α Forest*, an example of which is shown in figure 1.10. The density of lines in the forest depends strongly on redshift; at low redshifts these systems are rarely seen, but at high redshifts, they can grow so dense that they strongly can alter the appearance of the continuum blueward of emitter rest frame Lyα. The dependence of Lyα Forest density on redshift can be used as a cosmological tool to map gas density and

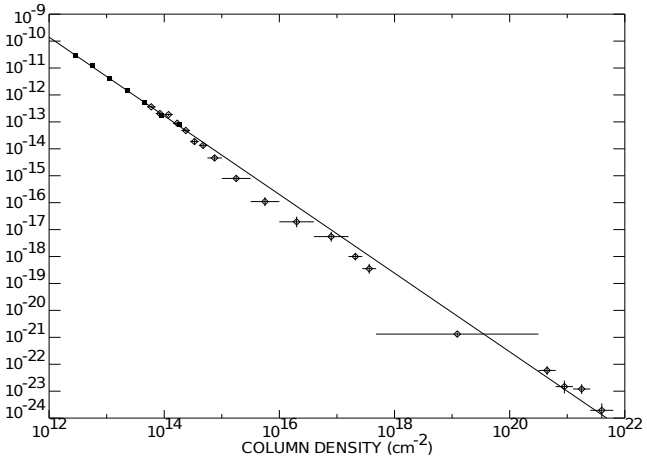

Figure 1.11: The number density of HI absorption systems, depending on their column density. While the lower- density systems are much more numerous, the majority of HI gas is found in Lyman Limit and DLA systems of column densities $\log N_{\rm HI} \gtrsim 17.2$. Image credit: Petitjean (1998), reproduced with the author's permission.

thus constrain Dark Matter models in the Universe at higher redshifts.

Systems of column density $N \gtrsim 10^{20}$ leave a broad, saturated absorption with broad damping wings in the spectrum of passing light. These are called *Damped Lyα Absorbers* (DLA) and are considerably more rare than Lyα Forest systems. Systems with intermediate column densities $10^{17} \lesssim N \lesssim 10^{20}$ are called *Lyman limit systems*. These typically are highly ionized (Petitjean, 1998) and often occur close to galaxies, making at least the most metal poor of them candidates for cooling flows of IGM accreting onto galaxy haloes.

Figure 1.11 shows the distribution in numbers of HI absorber systems of different column densities. The distribution is seen to be reasonably well approximated by a power law in N, although it dips somewhat below this law in the interval of $\log N \in [15, 20]$. Although the optically thin Lyman -α Forest system are by far the more numerous, the majority of cosmic HI is found in the LL and DLA systems. There has earlier been discussion of whether the DLA systems seen mainly in high-redshift quasar spectra were young galaxies or passive clouds of neutral hydrogen. This distribution shows that the DLA and LL systems constitute the main reservoir of neutral hydrogen and thus must be the source from which galaxies are formed and therefore with high probability must be galaxies themselves (Wolfe, 1986).

1.6 Lyman α in cosmology

1.6.1 Absorption

As photons from a source travel over cosmological distances, they are continually redshifted relative to the local rest frame. If they encounter a HI system along the way, this system will interact at the Lyα wavelength of the local rest frame, which will place a discrete absorption feature in the spectrum of the light source at a location blueward of the source's rest frame Lyα wavelength determined by the redshift between the two systems. Multiple systems at multiple locations will thus leave a number of lines, of depth and number density depending on their respective masses and average distance between them.

As we have seen above in Section 1.5, by far the most numerous systems are the ones of low column density. At redshifts of $z \sim 2$ and above, any given line of sight is likely to encounter such a large number of these systems that they leave a comb-tooth pattern in the spectrum blueward of the intrinsic Lyman α line, called the Lyman α Forest (see Sec. 1.5). The density and evolution in density of these lines can provide valuable insight to the large scale matter distribution in the Universe and its evolution. Substantial work has been done to use the Lyα Forest to constrain cosmological parameters (e.g. Lee et al., 2014; Seljak et al., 2006; Slosar et al., 2011; Weinberg et al., 2003). Likewise, the number and column densities of DLA systems at different redshifts can help constrain the evolution of galaxies, clusters and large scale structure. Analyses of dynamic mass and metallicity can help constrain nucleosynthesis and dust/metallicity at different epochs.

1.6.2 The Gunn-Peterson trough and the end of reionization

In the 1960's, it was suggested that the Lyman α line could also help determine when the epoch of reionization ended. Gunn and Peterson (1965) argued that a spectrum emitted in an neutral Universe would continuously have its light absorbed at local Lyα wavelengths while the spectrum itself gets continuously redshifted. Once the Universe was fully ionized, the light would be allowed to travel freely (barring encounters with absorbing systems of the types described above). The result would be a broad trough of zero flux of a width reflecting the redshift difference between the point of emission and the time of reionization being completed. Since the fraction of neutral hydrogen in the Universe needs only be $\lesssim \times 10^{-3}$ for absorption to be total, observation of such troughs would determine only the very end of reionization, but with fairly good accuracy.

It was not until the turn of the millennium that the first bona fide Gunn-Peterson trough was observed in a $z \approx 6.3$ quasar spectrum by Becker et al.

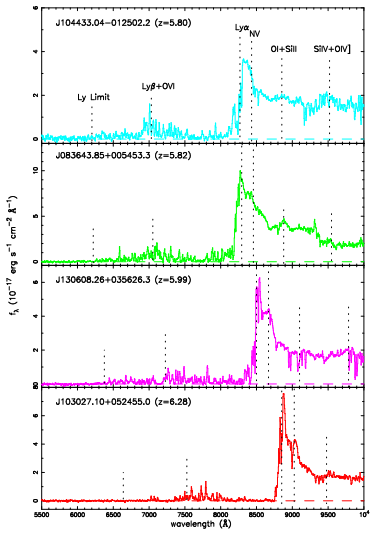

Figure 1.12: The first observed Gunn-Peterson trough, observed by Becker et al. (2001) in a quasar spectrum found in the SDSS (lower pane, red). For comparison, three other quasars are shown in the upper panels, in order of increasing redshifts. The rapid increase in absorption strength is interpreted by the authors as a sign that this redshift interval marks the end of cosmic reionization. Figure © AAS, reproduced with permission.

(2001). The group observed quasars selected for high redshift from the Sloan Digital Sky Survey and was at the time probing the maximum of observed redshifts, trying to find GP-troughs. In a paper the year before, the authors had observed a quasar at $z = 5.8$ which did *not* contain a GP-trough, setting a lower limit of the redshift of the end of reionization. In 2001, they pushed the limit further and observed four quasars in a redshift range of $z \in [5.8, 6.3]$. These spectra are shown in figure 1.12, which is taken from their paper. The only one of the spectra showing an actual GP-trough is Q1030+0524 at $z = 6.28$ showing in red in the lower panel. The residual flux blueward of Lyα grows so rapidly with decreasing redshift that the authors conclude that this quite narrow redshift interval indeed does mark the end of the epoch of reionization.

1.6.3 Constraining reionization with Lyman α Emitting galaxies

Studies of polarization of the Cosmic Microwave Background due to scattering on free electrons in the ionized IGM suggest that reionization of the Universe happened at a redshift of $z_{\mathrm{reion}} = 11.1 \pm 1.1$ (e.g. Hinshaw et al., 2013). As see above, measurements of Gunn-Peterson troughs in Quasar spectra suggest that reionization reached a point where the space averaged neutral Hydrogen

fraction $\langle x_{\rm HI} \rangle \sim 10^{-3}$ around $z \sim 6$. Note again that G-P troughs disappear only towards the very end of reionization, while the CMB scatters significantly as soon as a significant ionized fraction is present, so this discrepancy just reflects that the different methods probe different stages of reionization.

Quasars inhabit biased, overdense regions especially of the early Universe (Shen et al., 2007), regions which are more strongly ionized than the Universe as a whole. Therefore, quasar based estimates of the redshift of the end of reionization is likely biased towards higher values than are true for the Universe as a whole; the end of reionization has likely happened at $z \sim 5-6$, while it has begun some time at $z \gg 11$.

Studies of Lyα emitting galaxies have largely been in agreement with the results from quasar absorption line systems. Ouchi et al. (2010) compared a sample of 207 LAEs at $z = 6.6$ to other samples from the literature and concluded that the Lyα luminosity function decreases by $\sim 30\%$ at z between 5.7 and 6.6, while Ouchi et al. (2008) have concluded that there is no change in the Lyα LF for z between 3 and 6, despite substantial evolution in the UV LF at same redshifts, reflecting a growing stellar population towards lower redshifts. The sudden drop in the Lyα LF at $z = 6.6$ is therefore interpreted as attenuation by a neutral component of the IGM. However, Jensen et al. (2013) has shown that part of this change must be a change in intrinsic Lyα, otherwise the ionization fraction would have to have grown too steeply to be consistent with other observations. This dip in intrinsic Lyα luminosity could possibly be explained by the results by Hayes et al. (2011) as described in Sect. 1.2.5. The reported drop in $f_{\rm esc}^{\rm Ly\alpha}$ at redshifts $z \gtrsim 6$ is of course consistent with the rising coverage of neutral IGM patches at these redshifts, but besides this, the higher escape fraction of Lyα is probably due to lower HI optical depth, which will at some point allow for escape of ionizing photons, which in turn will not ionize hydrogen inside the galaxy and thus bring down the strength of recombination Lyman and Balmer lines.

In theory, Lyman α emission can be used to probe the evolution of x_{HI} even deeper through the EoR by studying the effect of the neutral IGM component on radiation from Lyα emitting galaxies. However, to do so, it is important to know how the ISM transforms the intrinsic Lyα line before it escapes the galaxy. The fraction of Lyα emitted from $z \gtrsim 7$ which reaches the telescope depends both on the emerging line strength and spectroscopic profile of the emission line and the absorption profile of the IGM, which in turn depends on average column density as well as geometry of the IGM, similar to what is the case in the ISM.

Figure 1.13 shows simulated, transmission curves averaged over a large number of sight lines to galaxies in hydrodynamic cosmological simulations at redshifts ranging from $z = 2.5$ to $z = 6.5$. Blueward of line center, the

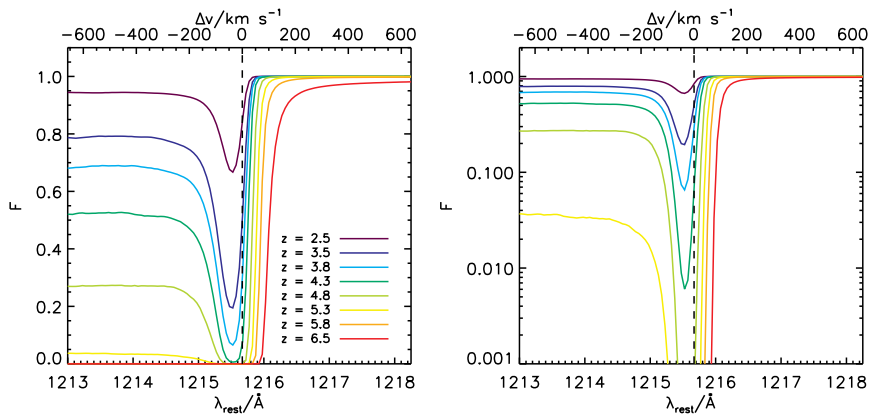

Figure 1.13: Simulated average transmission curves for the IGM at redshifts ranging from $z = 2.5$ to $z = 6.5$. On the blue side, the loss in transmissivity is due to the Ly α Forest which increases in density with redshift to eventually become G-P troughs. The dip around line center is due to overdense HI gas in the vicinity of the galaxy. Note the damping absorption setting in at high redshifts, broadening the range of low transmissivity well redard of line center. The two panels show the same transmissivity curves on a linear (left) and logarithmic (right) scale. Laursen et al. (2011), © AAS, reproduced with permission.

transmission coefficient is lowered according to the density of the Lyα Forest, which at high redshifts grows in density until eventually becoming a Gunn-Peterson Trough. Around line center, overdense HI gas gives an absorption dip. Note how at higher redshifts and thus higher HI density, damping wings in the absorption profile extend the range of low transmissivity well into the red side of the line. The curves in Fig. 1.13 serve as multiplicative envelopes for whichever Lyα line profile emerges from a given galaxy. By looking at Figs. 1.8 and 1.9 and imagining the transmission curves of Fig. 1.13 overlaid, it becomes evident that the fraction of the emergent flux that is transmitted through the IGM depends strongly on the shape of the line and the internal characteristics of galaxies that govern it, e.g. ISM outflow velocity, HI column density, possible backscattering, HI temperature etc. To correctly interpret observed luminosity functions etc. at these redshifts therefore requires a detailed understanding of these types of galaxies, which is exactly the scope of this work and the LARS project in general (see Sect. 3)

Hashimoto et al. (2013) measured the redshift of the Lyα emission peak in a sample of eight LAE galaxies at $z \sim 2-3$, and found a peak velocity of $v_{\rm peak} = 175 \pm 35$ km s^{-1}. Looking at the transmission curves of Fig. 1.13, these Lyα lines emerging from their galaxies of origin could reach us practically

unsuppressed in luminosity up to redshifts of $z \lesssim 6$.

The above transmission curves are averaged over many sight lines and therefore resemble what a homogeneous and homogeneously ionized medium would look like, but in reality, reionization is theoretically predicted to be patchy and inhomogeneous (e.g. Jensen et al., 2013), and observational evidence seems to support this (e.g. Pentericci et al., 2014).

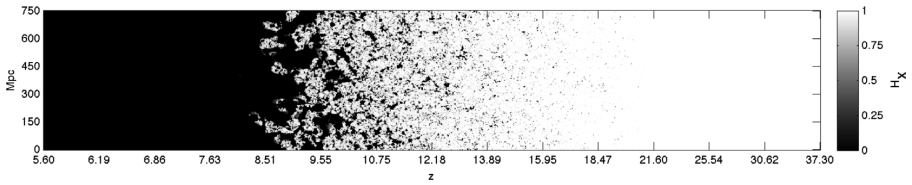

Figure 1.14: The predicted evolution of the ionization state of the IGM in a realistic model. White means neutral, black is ionized. Ionization starts in small bubbles which grow, merge and, towards the end of the EoR, can have an extent of several tens of Mpc. Image from Dijkstra (2014), reproduced with permission.

Figure 1.14 shows the predicted redshift evolution of the ionization state of the IGM from a realistic model. White means neutral, black means ionized. On the horizontal axis is redshift, the vertical axis shows spatial scale in comoving Mpc. Reionization begins in little bubbles localized around the first stars and galaxies under formation. These bubbles grow, merge and occupy an increasing fraction of intergalactic Space. At later stages of reionization, they can be several tens of Mpc across, before beginning to overlap so much that they are no longer well described as "bubbles".

Radiation from galaxies inside ionized bubbles of sufficient size will travel large distances before encountering the neutral IGM – distances that can be large enough that cosmological redshift has shifted the Lyα line so much towards the red that it can travel freely through the IGM. This will predominantly be the case for galaxies in coalescing clusters and other overdense regions, while field galaxies will occupy smaller bubbles which do not in the same way preserve Lyα flux. These relations can affect the apparent clustering of LAEs depending on the average HI optical depth of the IGM. Jensen et al. (2013) show how this can, with larger observed samples than currently available, be used to discern different reionization scenarios. Stark et al. (2016) find that bubble size seems to be correlated to galaxy luminosity, resulting in a further bias suppressing fainter galaxies and transmitting the radiation of brighter galaxies.

1.6.4 Lyman-α and Lyman Continuum

Lyman alpha emitting galaxies can not only be used to probe the epoch of reionization; they are also the main suspect for delivering the ionizing photons necessary for ionizing the early Universe. However, in the local and low-redshift Universe, the number of Lyman Continuum leakers is low, and their escape fraction not enough to account for the energy needed to complete reionization (see e.g. Jaskot and Oey, 2013, and references therein). The mechanisms by which Lyman Continuum radiation can escape gas-rich galaxies like the ones typically found in the early Universe is therefore a matter of intense research these years, and it has been suggested that both metal absorption lines (see e.g. Heckman et al., 2011, and citations therein) and the Lyman α emission profile (e.g. Verhamme et al., 2015, and references therein) can provide important indirect clues to whether a galaxy may be leaking Lyman Continuum. Especially the Lyα emission profile is coupled to Lyman Continuum in a profound way; the two kinds of radiation are both absorbed by neutral Hydrogen and thus they are expected to a large extent to escape through the same channels, if present[1]. We explore this connection between Lyα, Lyman Continuum and neutral metal absorption lines in Papers IV and V.

1.6.5 Other cosmology with Lyman α emission

Larger surveys have focused on using Lyα emission to map the large scale structure and constrain Dark Matter models by measuring clustering of galaxies at varying redshifts (e.g. Guaita et al., 2010; Kovač et al., 2007; Ouchi et al., 2004).

In a very ambitious endeavour, the Hobby-Eberly Telescope Dark Energy Experiment (HETDEX) is aiming to perform measurements of position and distance to a large number of Lyα emitting galaxies with the aim of measuring the Bary-Acoustic Oscillations in the Universe in an endeavour to constrain the Dark Energy equation of state.

[1] Although Ly-α is considerably more sensitive to neutral hydrogen than the ionizing continuum

2. The physics of atomic gas and ionized nebulae

In this chapter, I shall describe some basic astrophysical processes common in gaseous nebulae, which give rise to characteristic, observable features. These nebulae span a wide variety of physical conditions, from cold, neutral intergalactic gas clouds only visible in absorption; to hot, ionized, dense gas surrounding hot, new-formed stars or Active Galactic Nuclei, visible in strong emission. The work of this thesis has not been treating the cold, dense molecular nebulae, so they are also not discussed in this chapter. Whether observed in absorption or emission, the source of the UV and optical light that we mainly concern ourselves with in this work is predominantly young, hot stars in galaxies and, secondarily, AGN. Near the hot sources, atomic Hydrogen gas is ionized by young, hot OB type stars. Free electrons are then captured and recombine with the nuclei, cascading downwards through the energy levels while emitting a sequence of photons called *recombination lines*, as described in sect. 1.1. These hot nebulae also emit free-free (e.g. synchrotron) radiation, as well as bound-free radiation. These terms contribute to the overall continuum, but have not been important in the work of this thesis and shall not be discussed here. Besides recombination, free electrons also collide with, and in this way excite, bound electrons in atoms/ions, which can in turn decay back to their ground levels by emission of a photon. This is an important source of emission from metals (and an important cooling mechanism for the cloud); however, the lowest level in Hydrogen and Helium have too high energies to be collisionally excited by anything but the most extreme collisions, and thus the line emission of these atoms is dominated by recombination.

When photons travel through a gas system, those that have wavelengths corresponding to transitions in the atoms of the clouds are absorbed and later re-emitted in out of the original line-of-sight. Viewed along the line-of-sight to the source, these transitions will, in this simple case, be seen as darker absorption features in the spectrum. Viewed from other directions, the system will glow in the re-emitted light of these transitions. The typical case of almost pure absorption will be cold, intergalactic gas lit by a distant background source. Other systems will often display a more complex combination of emission and absorption feature, as well as more complex radiative transfer effects

like those described in Chapter 1.1.

This chapter describes some spectroscopic techniques to measure the physical properties of these systems, based mainly on their atomic transitions and resulting emission and absorption lines.

2.1 The Voigt profile

The optical depth around the resonance wavelength of given transition in a single absorbing system is a function of the column density N of the absorbing species and the interaction cross section σ of the given transition, as well as the internal kinematic and thermal properties of the system.

In a simplified situation, there is simply one, well defined energy of a transition, corresponding to a specific wavelength; the line profile would be a delta function. In reality, two things make this picture incomplete. *Firstly*, any system, be it absorbing or emitting, always has internal motion. This motion can be due to either small- scale (thermal) or large-scale (turbulence) motion. The difference between these lies in the relative widths of lines arising from different atoms in the same physical system: For thermal motion, energy equipartition will mean that lighter elements will have higher velocities than heavier elements, and thus lines arising from different atoms will have different width. In case of purely turbulent motion, all lines will have the same width, as the line broadening will be due to bulk motion of different regions of the system. Often, reality is a mix between the two. However, when it comes to the impact on each single line, there is no difference between the two: Both will tend to, on observable scales, average out and give a normal distribution of velocities, giving the line profile that arises from this effect a shape as a Gaussian function. *Secondly*, due to Heisenberg's principle, the finite life time of the upper level of a transition (and the lower, if this is not the ground state) means that the energy of the levels is not completely determined, but rather is a distribution. The probability $P(\lambda)$ for a photon of wavelength λ to resonate with the line is given by a Lorentz distribution.

The delta function of the simplified example exposed to these effects is mathematically described by a convolution of the Gauss- and Lorentz functions (since a convolution with a delta function just yields the original function). The result of this is a *Voigt* distribution. The shape of this is most often dominated by the Gaussian shape around line center, as natural broadening is a weak effect compared to thermal broadening in most practical cases. However, the Gauss profile drops off significantly faster in the wings than the Lorentz profile which is left to dominate far from the line center.

2.2 The Curve of Growth

The Voigt profile does, unlike its constituent distributions, not have a simple functional expression, and much research has been dedicated to how to efficiently compute it (e.g. Drayson (1976), Tepper Garcia (2006)). Since natural broadening is weak in optically thin systems, the Voigt line profile is often simply approximated by a Gaussian profile in such cases. In emission, this is a quite accurate approximation. In absorption, a Gaussian function subtracted from the continuum can be a good approximation for weak lines, but one should be more cautious here as the depth of the line approaches saturation.

Often, the Voigt profile is also approximated as the sum of a Gaussian and a Lorentzian, in cases where the wings are non-negligible. This is however not a very precise approximation, and in cases where a full multi-component, multi-line fit is carried out, it is preferable, if computationally feasible, to use a full Voigt profile.

An expression of the Voigt function in terms of observable parameters is given in e.g. Petitjean (1998) as:

$$H(a,u) = \frac{a}{\pi}\int_{-\infty}^{\infty} \frac{e^{-y^2}}{(u-y)^2+a^2}dy \tag{2.1}$$

where:

$$a = \frac{\lambda\gamma}{4\pi b} \tag{2.2}$$

and

$$u = -\frac{c}{b}\left(\left[1+\frac{v}{c}\right] - \frac{\lambda}{\lambda_0}\right) \tag{2.3}$$

with λ_0 being the laboratory wavelength of the transition, γ is the de-excitation rate of the upper energy level, b is the Doppler parameter of the absorbing gas.

The resulting line shape is then:

$$\tau(\lambda) = \tau_0 \times H(a,u) \tag{2.4}$$

$$= 1.498\times 10^{-2} \times \frac{Nf\lambda}{b} \times H(a,u) \tag{2.5}$$

and

$$I/I_0(\lambda) = e^{-\tau(\lambda)} \tag{2.6}$$

Here, $f\lambda$ is the *oscillator strength* times the wavelength, a measure of line strength.

The central panel of figure 2.1 shows a schematic of the dependence on column density of the Equivalent Width of an absorption line, the so-called *Curve of Growth*, for four different values of the *Doppler* or *broadening* parameter b. In the left side of the curve, in the optically thin regime, the line profile behaves largely like a Gaussian. The Equivalent Width of the line grows approximately linearly with column density N. An increase in Doppler broadening will be coupled to a decrease in line depth, leaving the line broader and shallower but with unchanged Equivalent Width, as is illustrated in the lower left panel of fig. 2.1. As N grows, the line grows saturated in the center, and a further increase in N will have little impact on EW – the CoG plateaus as is seen on the figure. However, an increase of b will in this regime have the effect of broadening the line which, due to the line being saturated, will not be followed by a decrease in line depth, so b can affect the equivalent width quite strongly in this regime. An illustration of this is given in the upper panel. How this reflects on the CoG is evident in the center panel; Where a change in b has little or no effect on the curve in the optically thin regime, it can have a strong impact on it in the middle phase. However, as N keeps growing, so does the impact of natural broadening and the importance of the Lorentzian wings, which at a certain point will create the broad damping wings seen in the lower right panel (note the difference in velocity scale from the top and lower left panels). A change in b in this regime will not have much impact on the EW because the broadening of the line it could bring has already happened due to the Lorentzian wings. However, an increase in N will now again lead to an increased EW, as this can make the damping wings deeper. The Curve of Growth is back in its roughly linear phase.

An important consequence of this is that at high column densities, the column density is reflected in the shape and depth of the line wings alone, since the center is strongly saturated, and because the line in this regime is roughly insensitive to broadening. Thus, even in case of residual emission, the wings, if present, are typically much wider than the emission feature and can be fitted to determine N_{HI} along the line-of-sight, as is done e.g. by Kunth et al. (1998).

2.3 Apparent Optical Depth method

Here follows a description of the *apparent optical depth* method, or *AOD*, as introduced by Savage and Sembach (1991) and utilized by e.g. Pettini et al. (2002) and Quider et al. (2009) and, in a version developed further, by Jones et al. (2013).

In case of an (idealized) well-behaved, non-saturated system of a simple

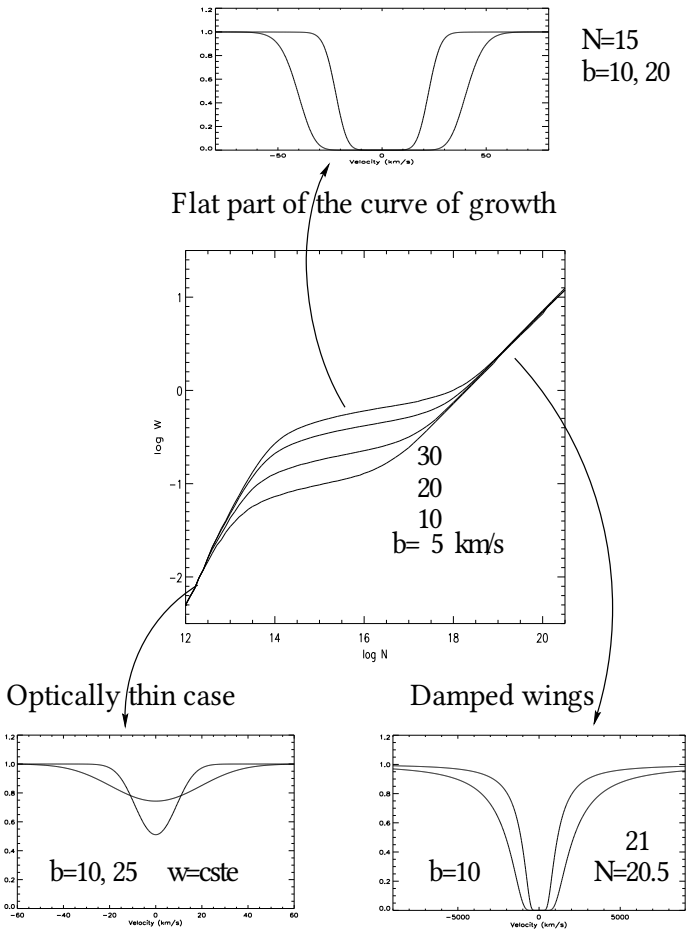

Figure 2.1: The Curve of Growth, illustrated. The central panel shows the dependence on column density of the Equivalent Width of an absorption line at different values of b. It clearly shows three regimes; an optically thin and an optically thick regime in which the dependence on b is weak, and an intermediate regime in which the dependence on $\log N$ is weak and that on b is strong. The upper panel shows the line of two different values of b in the intermediate regime, while the two lower panels illustrate characteristic behaviour in optically thin and thick regimes, respectively. Image credit: Petitjean (1998), reproduced with the author's permission

configuration of gas (e.g. a slab, a shell or similar), the optical depth of a system can be inferred in a simple way from the fraction of light that is transmitted and the fraction that is absorbed (see Savage and Sembach (1991)) as:

$$\tau_a(v) = ln(I_0(\lambda)/I(\lambda)) \tag{2.7}$$

The subscript a in τ_a indicates that this is "apparent", because this is the optical depth we infer from the observed intensity. In the idealized above case, this result is exact, but this configuration is not very realistic. Typically, a line of sight towards a source contains multiple absorbing subsystems, each contributing a component to the integrated line profile. The expected number of contributions can vary strongly, from a few in the outskirts of a galaxy lit from behind by e.g. a quasar, to greater numbers in the LOS to e.g. a GRB afterglow or star-forming knot in the central parts of a galaxy. These components can be very cool and dense, possibly making up components that are completely opaque but so narrow that they are smeared out when convoluted with the instrument resolution profile and thus appear as partly translucent, so called hidden saturation. If saturated components are present in the physical system, but not visible due to limitations in the instrument resolution or sensitivity, the apparent optical depth will in general *not* be equal to the physical optical depth of the system; the inferred optical depth will be lower for transitions with a higher value of line strength $f\lambda$. Thus, if two or more transitions of the same species are present in a spectrum, one can test for the presence of hidden saturation, while also giving multiple independent mappings of the column density per unit velocity bin.

If hidden, saturated components are present, the method provides a way of assessing how strong these components are, as the discrepancy in $N_a(\tau)$ between lines of different strengths will be stronger with stronger saturation. In practice; if no opaque components are present, multiple absorption features of the same species will show different equivalent widths in accordance with their difference in line strengths. If, on the other hand, all subsystems are completely optically thick, all the absorption lines will have the same depth everywhere when shown in velocity space; and anything in between will indicate a mixed state. The method is also useful for mapping the velocity distribution of dense, saturated systems, even in cases of quite poor resolution.

Compared to a classical multi-component Voigt-profile fitting approach, the AOD method provides less detailed information about the physical conditions in the absorbed system, but the information provided by such CoG analysis is quite heavily model dependent. For instance, a CoG analysis can precisely map column density, velocity and temperature of the absorbing subsystems and other information, but this information is strongly model depen-

dent. Maybe the weakest point in this technique is that it requires knowledge - or assumed knowledge - of the decomposition of a sometimes quite complex line profile, at least the number of components involved, which is not unique. The situation can be remedied somewhat, sometimes even a lot, if many lines of the same species or phase are present, in which case a lot of this degeneracy can be overcome, but such strong model dependency always casts a shadow of doubt on the results.

In comparison, the AOD method makes no assumptions at all about the configuration of the absorbing systems. Besides, where a classic line fitting and CoG analysis grows strongly in complexity with every added component in the line profile, the AOD method is carried out in the same way and yields the same information no matter how complex the line structure.

2.3.1 Covering fractions

The AOD method was originally constructed with a single line of sight to a point source in mind, but others later realized that it had a further advantage in the case of an extended source, e.g. a star cluster or star forming region in a galaxy, even if said source is not spatially resolved in the telescope. In this case, besides the above described effect of a narrow, saturated line component getting smeared by the instrument resolution profile, saturation can also be hidden in the shape of a completely opaque subsystem which only partly covers the background source. While the former kind of hidden saturation can be remedied with higher resolution, the latter can not.

We know that the denser neutral medium is often clumpy, and given the physical size of an extended source like e.g. a small number of star forming knots in the slit/aperture of a spectrograph, it is unlikely that this kind of sources should have dense, cold systems covering the entire source and creating hidden saturation as very narrow, opaque subsystems covering the entire source at uniform velocity, so when observing these or other targets where the typical size of dense subsystems is smaller than the physical extent of the background, a discrepancy in apparent optical depths between different lines of the same species can safely be assumed to be due to partial covering of the background source.[1]

The AOD method has been utilized by e.g. Pettini et al. (2002) and Quider et al. (2009) to compare the apparent optical depths of different lines in the same species to infer that at least part of the absorption features in their spectra, although individually being indistinguishable from multi component, optically

[1]Besides, a spectrograph like the COS actually has a good enough spectral resolution to not allow any physically realistic systems to “hide in poor resolution”.

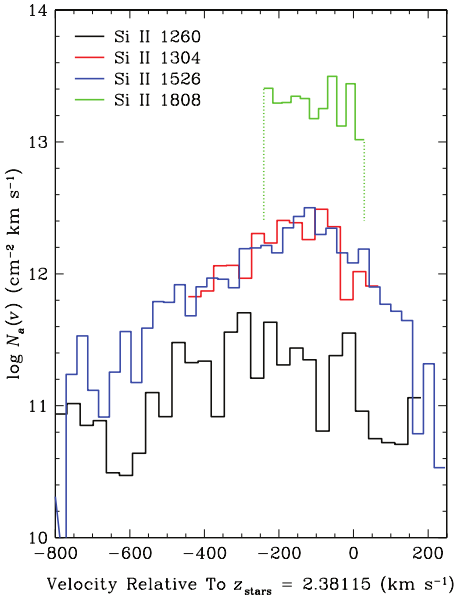

Figure 2.2: Apparent optical depths of four Si II transitions in a rest-frame UV spectrum of the Cosmic Horseshoe galaxy. The apparent optical depths span two orders of magnitude. Fig. 5 from Quider et al. (2009), reproduced with the author's permission.

thin lines, must in reality be made up of subsystems which are completely opaque but only covering part for the background source.

Figure 2.2 shows a plot of the apparent optical depths inferred from four different transitions in Si II in the strongly gravitationally lensed high-redshift Cosmic Horseshoe galaxy, from Quider et al. (2009). The four transitions span a range in $f\lambda$ of ~ 400. If no optically thick components were present, the apparent optical depth inferred from the four transitions would be the same (and equal to the true optical depth). This is clearly not the case; there is a strong discrepancy in apparent optical depths (note that the y scaling is logarithmic, the discrepancy is two orders of magnitude), revealing that the background source is only partially covered.

The method is further refined in Jones et al. (2013). Here, the author writes the intensity I_λ in a given wavelength interval as:

$$\frac{I}{I_0} = 1 - f_C(1 - e^{-\tau}) \tag{2.8}$$

where:

$$\tau = f\lambda \frac{\pi e^2}{m_e c} N = f\lambda \frac{N}{3.768 \times 10^{14}} \tag{2.9}$$

Here, I/I_0 is the intensity in terms of continuum intensity, f_c is the covering fraction of gas with velocity in the given interval. With n lines arising – now not only from the same species but from the same lower energy state – this can be solved as n equations in tow unknowns, in practice most easily done as a least-squares minimization problem, by letting f_c and N be the free parameters. The beauty of this is that this is valid (although not always useful) for any given velocity interval, as long as sufficient data is present. It is therefore possible, but this method, to actually create a mapping of column density and covering fraction of the given systems as a function of velocity. This is the version of the AOD method that we adopted for Paper I.

The nature of the covering fraction f_c computed by the above method may give rise to some confusion. Jones et al. (2013) caution that the figure obtained is the covering fraction of gas *with velocities within the given interval*. Lines in the galaxies studied often range in velocity width from $\sim$ 150 to $\sim$ 800 km/s; contributions from components with so strongly differing LOS velocities generally can not be expected to occupy the same projected space, and the largest covering fraction in an absorption line profile will strictly be a *lower limit* to the actual covering fraction at all velocities combined.

2.4 Absorption vs. scattering.

We have in the above treated the matter of atomic/ionic interactions with photons as a matter of absorption, in which a photon, when absorbed in an atom, is simply removed from the equation. This simplification is often a good approximation, but it is strictly speaking not correct, and in some cases, it is not a good approximation.

As is the case for Lyman α, the upper level of any transition has a finite life time, after which it will decay to a lower level by emission of a photon. This means that just as for Lyα, an absorption/emission event is in a sense a (perhaps very slow) scattering in a random direction. Unlike Lyα, however, it is not necessarily a *resonant* scattering, and even in the cases where it is, the much lower column densities of metals compared to HI means that the effect of radiative transfer in these lines is significantly less important than for hydrogen.

It has long been assumed in the treatment of absorption line spectra that this effect is indeed negligible. In case the distance between source and absorber is large, or the aperture covers only a small part of the interstellar and

circumgalactic medium, this is largely correct: much of the re-emitted radiation is (in analog with Lyα) transported out of the line of sight and, therefore, out of the slit/aperture before reemission, and does not pollute the measurements.

However, when the slit or aperture encompasses the majority of the neutral medium, as is often the case at high redshifts, a large fraction of the absorbed light is reemitted into the aperture and can add flux to an absorption, making it appear more shallow than the column density of the given species would do in the pure absorption case.

Prochaska et al. (2011) address this effect and its possible consequences by performing Monte Carlo simulations of radiative transfer in a set of selected lines in a simplified model of typical conditions in a star forming galaxy. The authors estimate the emergent line profiles emerging from a selection of lines. The authors also estimate the effect of the presence of a strong fluorescent line (which will decrease the effect of re-filling of the absorption trough, see discussion in Paper II), as do they discuss the impact of different aperture sizes, which can also mean a substantial difference in how strong this effect is. The authors stress that these models are not yet directly applicable, but further work has since been done by Scarlata and Panagia (2014), who crate a spherically symmetric outflow model with a velocity gradient strongly inspired by that of Prochaska et al. (2011) and simulate the radiative transfer effects on a subset of the Si II lines used for the analysis in Paper I (as well as in Jones et al., 2013) under different assumptions. They fit their model to a stacked spectrum and find a relatively good agreement with the absorption and fluorescent emission features in their spectra. However, more research is needed in order to reliably quantify the effect of radiative transfer in neutral metal lines.

2.5 The physics of nebular emission

The strength of an emission line depends on the strength of the mechanisms which populate its upper level. The main sources of energy in emission line nebulae are, as noted in the introduction to this chapter, photoionization and collisional excitation by free electrons. These in turn depend on physical properties like intrinsic stellar spectrum, temperature, matter density, chemical composition, etc. The dependence differs for different transitions; some transitions depend strongly on mainly one physical parameter, which can make them useful for measuring this parameter. In the following, some of the most common emission line diagnostics are described.

2.5.1 Dust reddening

When photons pass through a dusty medium, a fraction of them will encounter dust grains and be absorbed and its energy converted to vibrations in the grain (and eventually be re-emitted in the Infrared). The fraction of photons absorbed depends on wavelength, with longer wavelengths being less affected and having a lower probability of absorption. The result of this is a differential attenuation of the light, with the emerging spectrum being more luminous at longer wavelength compared to shorter wavelengths than the intrinsic one. When comparing spectral features with appreciable difference in wavelength, this needs to be taken into account and corrected for.

Besides wavelength, the exact effect of dust extinction and attenuation also depends on physical properties of the gas, as well as the geometric configuration of the gas and dust. A number of models have been developed, suitable for different kinds of systems like e.g. young starburst, high-mass quiescent Milky-Way-like spirals, Magellanic Cloud like systems etc.

Known intrinsic fluxes at different wavelengths can thus be used to determine how much dust is present in a system. One such known set of fluxes is the *Balmer decrement*, the ratio of Hα and higher order Balmer lines to Hβ. These ratios depend only weakly on density and temperature, and assuming *Case B recombination* (where the gas is optically thick in the Lyman series) and typical HII region conditions of $T_e \sim 10^4 K$ and $n_e \sim 10^2 \mathrm{cm}^{-3}$, as is considered typical for star-forming galaxies, the ratio of e.g. $H\alpha/H\beta$ is 2.87 (Osterbrock and Ferland, 2006). The deviation in observed line ratio from the intrinsic value can then be used to determine the amount of dust along the line of sight, and an appropriately chosen model can be invoked to correct for extinction at other wavelengths. $H\alpha/H\beta$ is often used because these are the strongest Balmer lines and have a large wavelength separation and thus a strong effect of dust reddening; however, other Balmer lines can be used and usually yield results in good agreement with this (Osterbrock and Ferland, 2006), making them a useful complement or replecement for $H\alpha/H\beta$.

2.5.2 Temperature and density

Temperature

Figure 2.3 shows a simplified diagram of the lowest energy levels of the doubly-ionized Oxygen atom. The ground state is split in three fine structure levels, two of which have transition from the first excited level, the $^1D_{2/1}$ state. Since both these transitions share the same upper level, the flux ratio of these two levels simply reflects the statistical weights of the lower fine structure levels or, in a different formulation, the A_{ki} Einstein coefficients of the transitions;

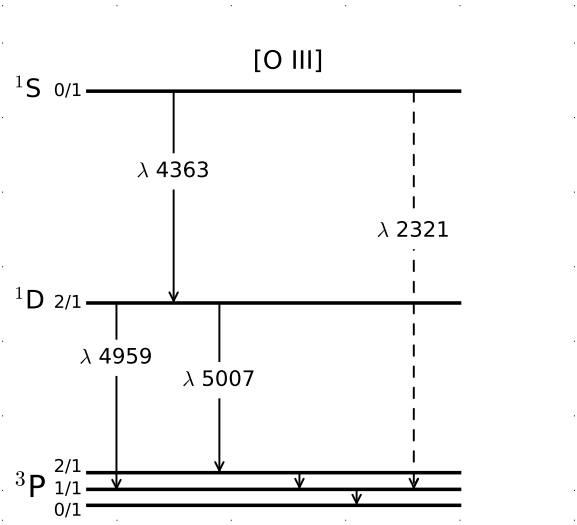

Figure 2.3: Energy level diagram for the lowest levels of O III. The distance between energy levels reflect their energy differences, but fine structure splitting is strongly exaggerated. Transition wavelengths are given in Å. Based on figure from Osterbrock and Ferland (2006)

and thus these always stay at a fixed ratio.

Another transition, from the second excited level, ${}^1S_{0/1}$ to ${}^1D_{2/1}$, is seen in the diagram, at $\lambda = 4363$ Å. The strength of this line depends strongly on the population of the upper level and thus the temperature of the gas. The fact that its wavelength is very close to the ${}^1D \rightarrow {}^3P$ transitions and Hβ makes it especially convenient for temperature measurements, as it means dust attenuation effects are modest, and all transitions can be observed simultaneously even on a detector with modest wavelength coverage.

The full dependence of the ratio $\frac{j_{\lambda 4959}+j_{\lambda 5007}}{j_{\lambda 4363}}$ on electron density n_e and temperature T_e is generally complicated, but for $n_e \lesssim 10^5 \mathrm{cm}^{-3}$, collisional de-excitation of the levels plays a negligible role, and with numerical values of collision strengths and transition probabilities, the relation:

$$\frac{j_{\lambda 4959}+j_{\lambda 5007}}{j_{\lambda 4363}} = \frac{7.90 \times e^{\frac{3.29\times 10^4}{T_e}}}{1+4.5\times 10^{-4} n_e/\sqrt{T_e}} \tag{2.10}$$

is a good approximation (Osterbrock and Ferland, 2006). The emissivity of these transitions, and the resulting line ratio as a function of T_e is shown in figure 2.4.

OIII emissivities in this figure are computed using the `pyneb` (Luridiana

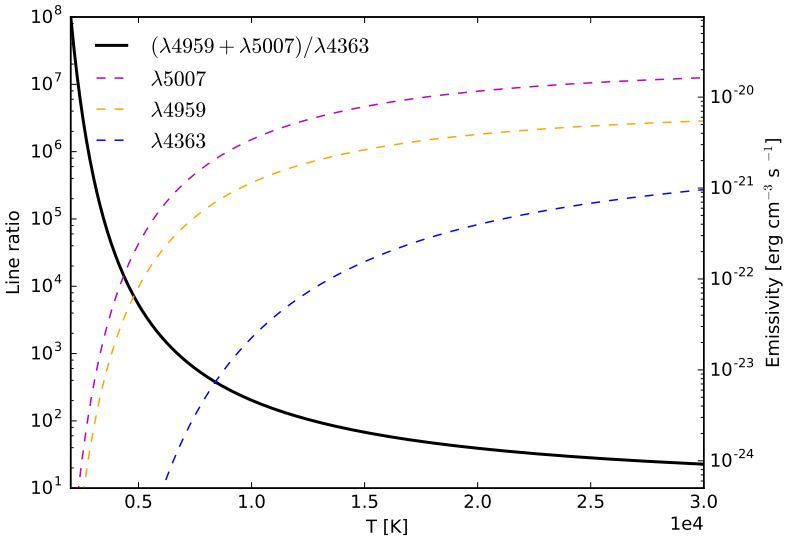

Figure 2.4: Emissivities and line ratios of the temperature sensitive diagnostic lines of O III. Emissivity is shown in colored-dashed lines towards the scale on the right, line ratio in full black towards the scale on the left.

et al., 2015) software package. They are shown in color-dashed lines, measured on the right-hand scale, while the line ratio is plotted in full black, towards the left-hand scale. The λ4959 and λ5007 are seen to follow a fixed ratio, while the λ4363 line is much fainter at low temperatures but grows closer in scale to the other lines as the temperature rises. This method of measuring electron temperature, and its extension to determine metallicity of the emitting gas (see Sect. 2.5.3) was used in Paper I, where it was used on archival SDSS spectra of the LARS galaxies, and in Paper III, where it was used to compute T_e for every single component in the model of ESO 338-IG04.

Other ions share a similar structure and similar line ratios to [O III] and can thus be used to compute T_e in a similar fashion, like e.g. [N II], [Ne III], and [S III] (Osterbrock and Ferland, 2006); however, only the [O III] lines have been used in this thesis.

Electron Density

Other ions have an energy level structure which makes them more sensitive to the density of free electrons, n_e, in the following way.

In the diagram in Fig. 2.5, the lowest energy levels are sketched of the two structurally similar ions, [O II] and [S II]. Again, the distance between

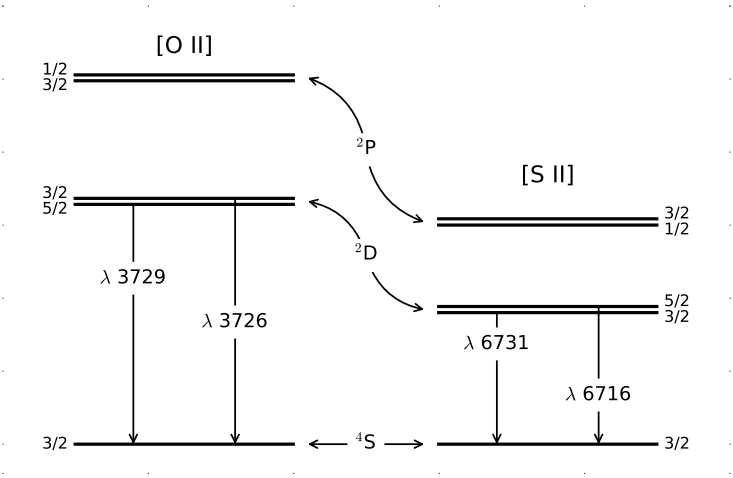

Figure 2.5: Diagram of the lowest energy levels of O II (left) and S II (right). The distance between energy levels reflect their energy differences, but fine structure splitting is strongly exaggerated. Transition wavelengths are given in Å. Based on figure from Osterbrock and Ferland (2006)

main energy states reflects the energies of the transitions, while fine structure splitting is strongly exaggerated. Unlike the [O III] family of ions, in these, the ground levels is a singlet, while the first excited level is a doublet. As a result of this, the intensity ratios of these lines are governed by the relative populations in the fine structure levels of the upper ^2D states of these lines. In the low density limit, this is simply governed by the statistical weights of these levels, but as the electron density grows, the populations of the ionic energy levels begins to be affected by collisional excitation and de-excitation until, in the high density limit, $n_e \to \infty$, the electrons are completely thermalized and the levels reach a Boltzmann ratio of populations (Osterbrock and Ferland, 2006).

As an example, consider the [O II] $\lambda\lambda 3726, 3729$ line ratio. In the low-density limit, where the typical time between collisions is much shorter than the typical time between spontaneous emission, such that a free electron is very unlikely to collide with an already-excited, bound electron. In this case, electrons only leave their respective levels by emission of a photon, such that the line ratio is simply the ratio of the statistical weights of the levels of the doublet; in this case $\lambda 3729/\lambda 3726 = 1.23/0.82 = 1.5$ (Osterbrock and Ferland, 2006, table 3.7), with collisional rates evaluated at $T = 10^4 K$, a typical value for ionized nebulae. However, as the density grows larger, collisions happen more often, and so collisional excitation and de-excitation of the lev-

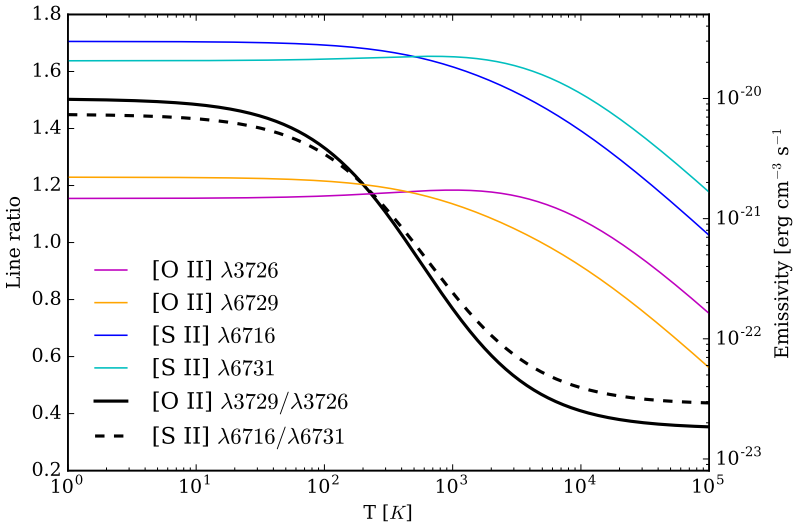

Figure 2.6: Line emissivities for the density sensitive S II and O II doublets as a function of N_e, as well as the diagnostic line ratios. Ratios are shown on a linear scale marked on the left, emissivities on a logarithmic scale shown on the right.

els becomes more frequent. From which level in the doublet a photon decays to the ground state thus depends on both the statistical weights (reflecting to which level an electron is more likely to be excited), and the spontaneous emission coefficients, reflecting how likely the electron is to decay to the ground level before being de-excited by a new collision. Thus, to a first approximation (Osterbrock and Ferland, 2006):

$$\frac{j_{\lambda 3729}}{j_{\lambda 3726}} = \frac{n\left[^2D^0_{5/2}\right]}{n\left[^2D^0_{3/2}\right]} \frac{A_{\lambda 3729}}{A_{\lambda 3726}} = \frac{3}{2}\frac{3.6\times10^{-5}}{1.6\times10^{-4}} = 0.34 \tag{2.11}$$

The value of n_e beyond which collisional (de-)excitation is no longer negligible is called the *critical density*. In the case of the [O II] $\lambda\lambda$3726, 3729 doublet, the densities are $n_e = 1.5\times10^4$ and 3.4×10^3, respectively (Osterbrock and Ferland, 2006, table 3.15).

The `pyneb`-computed emissivities for the relevant lines and their ratios are shown in Fig. 2.6. As in fig. 2.4, emissivity is shown in colors towards the scale on the right, while the line ratios are shown in black with scale marked on the left. These graphs are computed from a full, numerical treatment of the atoms, including excitations to higher levels and downwards cascading etc. too complex to be treated here.

Below (above) the critical densities, the diagnostics can only give an upper

(lower) limit of n_e. Note also that the two line ratios are reversed: for Oxygen, the bluer line is in the denominator, while for Sulphur, it is the redder line. In both ions, the $^2D_{5/2}$ level has a larger statistical weight than the $^2D_{3/2}$ level. However, as illustrated in fig. 2.5, this level has a lower energy and thus longer transition wavelength in Oxygen, and vice versa in Sulphur.

It should also be noted that the graphs shown in fig. 2.6 are based on collision rates/statistical weights evaluated at $T_e = 10^4 K$; like in eq. 2.10, the full dependence is also on temperature, most strongly on the $n_e/\sqrt{T_e}$ term. This temperature dependence varies quite slowly in the typical temperature range of H II regions, and often an approximate T_e estimate is enough to get a good approximation to n_e; however, for a more precise and robust computation, software like `pyneb` has iterative methods to simultaneously determine T_e and n_e when line diagnostics for both are available.

2.5.3 Metallicity from recombination and forbidden lines

Direct method from T_e

In Hydrogen (and Helium), the first excited level has a high enough energy that collision with a free electron is unlikely to be able to excite the electron. Many heavier elements, however, have energy levels of only a few eV; low enough to be easily excited by such a collision. The electron can then be de-excited either by another collision, or by spontaneous emission of a photon. This is an important cooling mechanism for gas, and thus systems of high metallicity can cool much more efficiently than low metallicity systems.

The relative abundances of heavy elements can be found by comparing the strengths of collisionally excited, "forbidden" lines in ions of these elements, and the strength of the Hydrogen recombination lines. However, the rate of collisional excitation of the bound electrons in these heavy ions is temperature dependent, so in order to convert the line ratio into an abundance it is necessary to know the temperature of the gas in question.

The abundance of doubly-ionized Oxygen to ionized Hydrogen can thus be found directly by measuring the temperature and the [O III]$\lambda 5007/H\beta$ or [O III]$(\lambda 4959 + \lambda 5007)$ ratio. The relation is (Draine, 2011):[1]

$$\frac{n([\mathrm{O\ III}])}{n(\mathrm{H\ II})} = C \frac{j_{\lambda 5007}}{j_{\mathrm{H}\beta}} T_4^{-0.37} e^{2.917/T_4}, \tag{2.12}$$

[1]There is some confusion as to whether to name the transitions by their air or vacuum wavelengths, and thus whether the [O III] $^1\mathrm{D}_{2/1} \rightarrow ^3\mathrm{P}_{2/1}$ transition has wavelength 5007 or 5008 Å. I have altered Draine's notation to comply with the standard adopted in the rest of this thesis.

where C is a constant factor encoding, among other things, the transition energies, their Einstein coefficients, the [O III] collision strength, and the recombination rate of Hβ (see Draine, 2011, for a full description); and T_4 is the electron temperature in units of $10^4 K$. The ratio $n([\text{O II}])/\text{H II}$ can be found from the [O II]$\lambda\lambda 3726, 3729$ lines from a similar formula (derived from eq. 18.9 in Draine (2011)). Neutral Oxygen has an ionization potential very close to that of Hydrogen, and the ionization potential for O III $\rightarrow$ IV is high enough that only a very hard spectrum will create a significant fraction of triple-or-higher ionized O (Izotov et al., 2006, see e.g.), so O II and O III are the dominant species of Oxygen in emission nebulae, and knowing their abundances gives a very good approximation to the total O/H abundance.

More generally, the total abundance of an element can be computed as just the sum of the abundances of its different ionization levels. Often, however, only one or two ions of an element are observed in sufficient detail, and one must employ so-called Ionization Correction Factors, such that Luridiana et al. (2015):

$$\frac{n(X)}{n(H)} = \sum_{\hat{\imath}} \frac{n(X^{\hat{\imath}})}{n(H^+)} \times \text{ICF}, \tag{2.13}$$

where the index $\hat{\imath}$ runs over the observed ions only. These ICFs summarize models, assumptions and empirical relations about ionization degrees, nebula structures etc., and are often specific for a given kind of object like e.g. an H II region. The ICFs relevant for this thesis are for O in H II regions and are by Izotov et al. (2006), incorporated in `pyneb`, although as mentioned above, the corrections necessary for Oxygen with both [O II] and [O III] measured are small.

Empirical strong-line methods

While the direct T_e based method for determining metallicity of a nebular system is useful and quite accurate, its dependence on a sufficiently strong auroral [O III] $\lambda 4363$ line often makes it impractical. Firstly, at typical temperatures for an ionized nebula of $\sim 10^4 K$, the line is intrinsically quite faint and thus only detectable at low redshifts in the local Universe. Furthermore, the higher Oxygen abundances, which could otherwise naively make the line stronger, means more efficient cooling and thus lower temperatures and a weaker of completely absent auroral line.

There is therefore great interest in finding ways to determine abundances which depend only on strong emission lines which can be reliably detected at a large redshift and metallicity range. There are no direct ways to measure abundances directly from strong lines alone, due to the temperature/abundance

degeneracy, but a number of empirical relations and calibrations have been developed over the years (e.g. Marino et al., 2013; Pettini and Pagel, 2004; Pilyugin, 2000, 2001; Pilyugin et al., 2012; Skillman et al., 1989; Yin et al., 2007). These diagnostics are usually found by measuring a combination of strong emission lines reflecting some physical property which tends to correlate with metallicity, and then calibrate this correlation against either direct T_e based measurements, although some calibrate them by theoretical photoionization models (e.g. Kewley and Dopita, 2002; McGaugh, 1991).

One particularly popular strong-line diagnostic has traditionally been the **R_{23}** method, based on the quantity:

$$R_{23} = ([\text{O II}]\lambda\lambda 3726,3729 + [\text{O III}]\lambda\lambda 4959,5007)/H\beta \tag{2.14}$$

This indicator was suggested for use with high-metallicity galaxies by Pagel et al. (1979), and Skillman et al. (1989) showed that it was also useful for low-metallicity galaxies with no detected auroral lines. However, when R_{23}-derived abundances are plotted against T_e, it is found that the function is two-valued, and the turnover happens at $12+\log(\text{O/H}) \approx 8.2$, which is a quite typical value for the local starburst galaxies analyzed in this work, and this is a well known problem in many contexts. The diagnostic has also been found to consistently overestimate the abundances compared to the directly measured values (e.g. Kennicutt et al., 2003; Pilyugin et al., 2006) by ~ 0.5 dex. Yin et al. (2007) show that this discrepancy can be made considerably smaller by taking into account the ratio of doubly and singly ionized Oxygen, encoded in the parameter $P = \text{OIII}/(\text{OII}+\text{OIII})$. The scatter is largely unchanged by this, and it does not solve the problem of the double-valued correspondence between this and the direct method, which renders this method impractical at values of $12+\log(O/H) \gtrsim 7.95$.

Another emission line ratio which can be used is **N2** = [N II]/Hα (e.g. Denicoló et al., 2002; Pettini and Pagel, 2004; Storchi-Bergmann et al., 1994). Nitrogen is primarily produced in intermediate and low mas stars (Yin et al., 2007), which means Nitrogen abundance grows with the long-term enrichment of the interstellar gas, and the [N II]/Hα line ratio correlates with metallicity up to $12+\log(\text{O/H}) \gtrsim 9$ (above Solar metallicity), at which point the metal cooling gets so efficient that the line strength begins declining again. The N2 method is powerful, because the lines are so close, that dust attenuation is not an issue, and the requirements to spectrograph wavelength coverage are minimal, as well as for being useful for a much wider range of metallicities than the *R*23 method. However it also has weaknesses: it has a quite strong scatter and, perhaps more importantly, it is an indirect measure of O abundance, since no Oxygen lines actually enter the computations. This means that it is

sensitive to changes in N/O ratio, and thus can be misleading. The scatter is improved by Yin et al. (2007) by again including the factor P in the analysis, but it comes at the cost of needing more lines observed, and depending on an accurate dust dereddening. Results computed by this method are included in Paper I, Table 1.

Based on larger samples of T_e computed abundances, as well as strong-line-based abundances based on a combination of Oxygen, Nitrogen and Sulphur lines (ONS-calibration), Marino et al. (2013) improve the calibration of the N2 method, reduces the scatter and prescribes a linear relation between the N2 factor (log([N II] / Hα)) and the logarithmic abundance, based on the N2 factor alone, regaining the power of the original N2 based method. Results based on this method are included in Paper III, figs. 10–12 and Table 3.

A third, powerful method is based on the quantity **O3N2** (Alloin et al., 1979; Pettini and Pagel, 2004; Yin et al., 2007):

$$\mathrm{O3N2} = \log\left(\frac{[\mathrm{O\ III}]/\mathrm{H}\beta}{[\mathrm{N\ II}]/\mathrm{H}\alpha}\right) \tag{2.15}$$

Like the N2 method, this has its strengths and weaknesses. It depends on ratios of lines which are very close together, meaning that the effects of dust reddening are small even in uncorrected spectra; and that the necessary lines can be observed in two settings even with a spectrograph of very low wavelength coverage. The inclusion of doubly-ionized Oxygen vs. singly-ionized Nitrogen also encodes some information about the ionization and excitation state of the gas. In earlier adaptations like e.g. that of Yin et al. (2007), it has a larger scatter than the N2 method, but it does not rely on assumptions about N/O. It is considerable more scattered than the N2-P method, but is much less demanding wrt. wavelength coverage, and does not require dereddening. This method in the incarnation by Yin et al. was used in Paper I, table 2.

Like the N2 method, O3N2 was revisited by Marino et al. (2013), and here, the new calibration data sets paid off; a robust linear fit was made in O3N2 and $12+\log(\mathrm{O/H})$, and the scatter was reduced strongly. Results based on The Marino et al. (2013) incarnation of this method are reported in Paper III, Figs. 10–12, and Table 3.

In Paper I, we used these techniques mainly to determine the total metallicity and ionization of each of the LARS galaxies. In Paper III, we used those in a much more extended manner to describe the galaxies in detail, identifying dense, high-ionized and sparse, low-ionization regions and reveal what appears to be a low-luminosity AGN or accreting Intermediate Mass Black Hole which has been undetected so far, its light drowned out by the strong, surrounding starburst.

3. The Lyman Alpha Reference Sample

The Lyman Alpha Reference Sample is a sample of 14 galaxies at low redshifts selected from the GALEX and SDSS catalogs. The galaxies are selected for their high equivalent width of H$\alpha > 100$ Å to ensure that the galaxies are indeed actively star forming and thus also produce a significant amount of ionizing photons, to make sure Ly α is indeed produced in the galaxies. To exclude galaxies with an AGN component, galaxies with a FWHM(Hα) > 300 were excluded from the sample. Galaxies in the sample have redshifts within a range from $z \approx 0.02$ to $z \approx 0.2$. The range was chosen to keep Lyα inside the relevant bandpass of the SBC, while also keeping Lyα well clear of the geocoronal line. The selection cut of high EW(Hα) yields a collection of mostly compact, irregular galaxies, while eLARS, with a lower Hα cut, contains a larger fraction of spirals. The LARS galaxies span a range in luminosity, masses, Lyα escape, and metal abundance, all of which relate to evolutionary stage. One of the goals of the sample is to test how large a fraction of these galaxies (believed to resemble the general population of small, star forming galaxies in the early Universe) would even be detectable at high redshifts, which of course makes it important to do away with as many kinds of selection bias as possible.

The sample has later been extended by 28 more galaxies, "eLARS" (the extended LARS), selected by the same criteria as the original sample but with lower Hα equivalent width and thus lower intrinsic Lyman α production; as well as a small sample of 5 ultraluminous infrared galaxies (ULIRGS). Analysis of these new subsamples is still ongoing and has yet to be published at the time of writing this.

The LARS galaxies have been observed with a number of instruments and at many wavelengths and techniques, including multi-band imaging with the HST ACS Solar Blind Channel and the Wide Field Camera 3, optical archival spectroscopy from SDSS, IFU spectroscopy with Calar Alto PMAS, single-dish 21 cm observations with the Green Bank Telescope, radio interferometry at 21 cm with the Karl Jansky eVLA and the Giant Metrewave Radio Telescope.

The first observations of LARS, multi-band imaging with HST, published in Hayes et al. (2013), showed that the Lyα halos, where present, are mor-

phologically different from and extend significantly further out than the stellar population and the recombination nebulae, showing that significant resonant scattering of Lyα is indeed happening in the neutral gas of these galaxies. The effect does not correlate with Lyα luminosity, but does correlate with dust content. The data hint that a low dust content is a necessary, but not sufficient, requirement for Lyα photons to scatter far away from their place of origin and produce extended Lyα halos. This confirmed that Lyα resonant scattering is indeed an important and significant process, and also hints that the Lyα radiative transfer in galaxy haloes is a multi parameter problem.

In Hayes et al. (2014), this analysis is continued in greater depth. The Lyα halos are found to be more extended, but with a flatter radial profile, than the general UV profile, meaning that the EW of Lyα is underestimated at small central apertures. The flat profile also means the Lyα radiation is distributed over a larger projected area with a lower surface density, which could lead to underesimation at high redshifts. However, for the sample galaxies, this was found to be a significant problem for only a couple of galaxies. Ten of the galaxies were found to be equivalent to high-z Lyman Break galaxies, and six would be selected at high-z LAE surveys with a typical cutoff of EW(Lyα) $\gtrsim$ 20 Å

Guaita et al. (2015) characterized and studied the morphology of the LARS galaxies and found, in agreement with Hayes et al. (2014), that the galaxies in general shared characteristics with local Lyman Break Analogs and redshift $2 < z < 3$ star forming galaxies often found as Lyman Break galaxies. It was also found that they shared some characteristics with the most massive high-redshift LAEs, but are not characteristic of these. The sample is dominated by merger-like morphologies. It was also found that the LAEs among the sample were more compact than the non-LAEs with lower EWs. This was true even when regridded to an angular scale typical of would be observed at high redshifts, meaning that if this is generally true for LAEs, a larger fraction of them are likely to be detected at high redshifts than if they were less compact.

The neutral gas content of the sample has also been studied directly in the HI 21 cm spin-flip transition with the single-dish Green Bank Telescope, and the galaxies that showed sufficiently strong detections here have been observed in interferometry with the Karl I. Jansky Very Large Array at various configurations, of which the earliest results, together with the GBT results, have been published by Pardy et al. (2014). This allowed publication of directly measured gas masses and line profiles for the sample galaxies (except LARS 11-14 which were not detected with GBT), as well as a mapping the distribution and motion of the gas on scales much larger than the optical images of the galaxies. It was found that the HI mass anticorrelates with $f_{\rm esc}^{\rm Ly\alpha}$, as expected from theoretical studies by e.g. Laursen et al. (2009b), and fits with the finding

of Hayes et al. (2014) that Lyα properties correlate with total galaxy mass.

Herenz et al. (2016) report integral field spectroscopy with the Potsdam Multi-Aperture Spectrophotometer (PMAS), from which the velocity field was derived and mapped from the Hα emission. Velocities, velocity dispersion and shear velocity are found anbd compared, showing that the LARS galaxies have comparatively high velocity dispersions and low shear velocities, reflecting systems with a high degree of turbulence and relatively little rotation. Five of the galaxies are velocity dispersion dominated, reflecting the conditions in high-z starforming galaxies, but in contrast to local spirals. The high dispersion systems are also the ones with the highest Lyα EW and escape fraction. These results suggest that high turbulence creates ISM conditions favorable for Lyα escape.

In Rivera-Thorsen et al. (2015) – Paper II in this thesis – we investigate the kinematic and geometric properties of the neutral gas along the line of sight to the brightest star forming know in each galaxy, with special interest in measuring the presence and possible velocity of outflowing winds and to probe the clumpiness/porosity and of the medium. It is the first ever study to couple observations of local ISM kinematics with large-aperture observations which can reveal properties of global Lyα radiative transfer. We found, among other things, that the kinematics described in sect. 1.1 does indeed play a role: Lyα escape coincides everywhere with bulk outflowing gas, although other factors like e.g. increased line with or high dust content could still suppress the radiation even with a significant outflow. Furthermore, we found that Lyα escape coincided with the lower maximumvalues of f_C as described in Sect. 2.3.1, suggesting that Lyα escapes more easily through such channels of low HI density. No direct correlation was found between Lyα escape fraction and any other single quantity; the data confirmed that Lyα escape is indeed a multi parameter problem. It was however found that Hα EW correlated strongly with $f_{C,\mathrm{max}}$, which we interpreted as the strong star formation feedback from the high-EW(Hα) systems giving rise to Rayleigh-Taylor instabilities in the surrounding medium, creating channels of low resistance to Lyα escape. This interpretation is in agreement with observations by Hayes et al. (2014), where it was found that locally enhanced Lyα coincided with filamentary structures in Hα, suggesting the same.

Work is still ongoing with LARS and the extended sample; papers are underway presenting detailed modelling of the Lyα profiles and comparison to radiative transfer models (Orlitová et al., in prep.); higher spatial resolution configuration interferometric imaging of HI in 21 cm (Cannon et al., in prep.), and more.

4. Summary of papers

The papers are here grouped thematically. However, when it comes to the observational techniques and analysis methods, papers I and III share many similarities, as do Papers II, IV and V.

4.1 Papers I and II: The Lyman Alpha Reference Sample

These two papers are part of a series of papers about the Lyman Alpha Reference Sample, number 1 and 5 in the series. The purpose of this sample, as described in Sect. 3, is to understand the radiative transfer and escape of Lyman α radiation from its production sites in the hot, star forming interiors of galaxies, and into intergalactic Space, by studying a sample of galaxies which are all selected for their large production of Lyα photons, but with observed Lyα ranging from bright emission to deep, broad absorption. The sample is studied by multiple methods, in wavelengths ranging from X-rays to 21 cm. radio emission, an effort to understand the internal dynamics and the interplay of factors regulating Lyman α radiative transfer in as great detail as possible.

Paper I, first author Göran Östlin, presents the Lyman Alpha Reference Sample: its purpose, context, design, methodology, and sample selection; and demonstrates the capabilities of its techniques exemplified by the sample galaxy LARS 1, also known by the name Markarian 259. The paper discusses sample selection criteria, Imaging and reduction techniques, and presents the sample as seen in SDSS imaging and spectroscopy, the latter being my contribution to the paper, as discussed in Sects. 2.5.2 and 2.5.3. The paper presents HST broad-band imaging of the galaxies (the line emission maps are computed and presented in Hayes et al. (2014)), and then proceeds to present some of the techniques developed for the image analysis presented in Hayes et al. (2014), and the results of these applied on LARS 1, also known as Markarian 259. Also preliminary HST-COS FUV spectroscopy is presented with a preliminary kinematic analysis of the ISM lines, and a fit of the Lyα line to a model based on those in Verhamme et al. (2006), although a more ind-depth spectroscopic analysis of the ISM lines was preserved for Rivera-Thorsen et al. (2015) (Paper II), and of the Lyα line for Orlitová et al. (in prep.).

In Paper II, we analyze data from the LARS COS campaign, obtained

either by observation campaign 12583 (PI: M. Hayes) or as archive data from campaigns 11727 (PI: T. Heckman), 11522 (PI: J. Green) and 12027 (PI: J. Green). We determined systemic redshifts from archival optical spectra from the SDSS Data Release 7. From these, we fitted several strong, nebular emission lines to single Gaussians, derived their individual redshifts with respect to laboratory wavelengths tabulated at NIST[1] and computed an average weighted by the uncertainties obtained from the fitting software. The same fits were used to determine metallicities for the galaxies, which were later used to recalibrate the continuum subtraction routines of (Hayes et al., 2014). The metallicities were found through multiple methods where applicable, as described in Östlin et al. (2014). The SDSS spectrum analysis was presented in Östlin et al. (2014), which is not included in this thesis.

We normalized the data around a list of low- and high-ionization metal absorption lines and interpolated them to a common velocity scale. We then computed an average line profile from the normalized and regridded lines of Si II $\lambda\lambda$ 1190, 1193, 1260 and 1304, as well as O I λ 1302 and C II λ 1334. This line is in the remainder of the work used as a proxy for the LIS phase. The same was done for the three available lines of Si IV $\lambda\lambda$ 1122, 1393 and 1402, taken to represent the HIS phase. These were plotted together for comparison, to test for systematic offsets in velocity and depths. It was hypothesized that the HIS lines should show slightly higher velocities, as they mainly originate at the interface between the hot, ionized gas and the cool, neutral gas, where the former rams into the latter.

The covering fractions per velocity step of the Si II lines were then mapped by the method mentioned in Section 2.3.1. These were found to generally agree well with the averaged profile, which we interpret as the observed systems being dominated by optically thick components with partial covering. The averaged profile was then also adopted as a proxy for the covering fraction profile; it shows less scatter and therefore was better suited for locating flux density minimum, FWHM and other characteristics, and we deemed it likely that the scatter in the computed covering fraction maps was due to the method's vulnerability to noise and other uncertainties in measurement.

From the averaged profile, a number of characteristics was then measured, which are described in detail in sect. 3.5 in Paper I. Among the most important were the integrated central velocity, defined as the velocity which has half the absorbed area on each side; the Lyman α peak velocity; the full width at half minimum and the velocity at 95% integrated absorption, defined as the velocity which has 95% of the integrated absorption on it's red side. This serves as a measure of the maximum velocities of LIS subsystems.

[1] http://www.nist.gov/pml/data/asd.cfm

We find that systems with Lyα above a few percent also consistently show LIS outflow velocities of $\gtrsim$ 50–100 km s^{-1}, in agreement with earlier studies of e.g. Kunth et al. (1998) and Wofford et al. (2013). Balmer decrement is weakly correlated with global Lyα escape. We find that all galaxies with a Lyα escape fraction $f_{\rm esc}^{\rm Ly\alpha} \gtrsim 0.05$ also have a maximum covering fraction $f_C^{\rm Ly\alpha} \gtrsim 0.9$. Furthermore, we discovered, quite unexpectedly, a strong correlation between maximum velocity-mapped covering fraction and $W_{\rm H\alpha}$. We propose an explanatory model, in which stellar and SN feedback gives rise to Rayleigh-Taylor instabilities in the outflowing medium which cause it to fracture into disjoint clumps with individual velocities spread around a mean. This we suggest as an amendment to to an evolutionary model suggested by Tenorio-Tagle et al. (1999) with elaborations by Mas-Hesse et al. (2003).

Alternative explanations for this correlation have been suggested, of which the following should be mentioned. *Firstly*, intrinsic clumping: Hα is a tracer of SSFR, and more stars are formed in an intrinsically clumpy medium. (A. Adamo, private communication.) *Secondly*, Radiative transfer effects as described in Section 1.4. This would imply that the observed fragmentation of the neutral medium would only be apparent. RT effects could re-fill the absorption trough of an optically thick absorption line from a fully covering medium, giving it a false appearance of porosity. This effect is stronger when a large fraction of a galaxy's neutral medium is seen through the aperture (Prochaska et al., 2011; Scarlata and Panagia, 2014). This would mainly be the case for compact galaxies, which are also well known as hotbeds of star formation and thus will tend to show a higher equivalent width that larger galaxies. (C. Scarlata, private conversation.) More research is needed in order to establish whether this poses a problem for the AOD method.

4.2 Paper III: Warm ISM in local starbursts

Paper III is based on a set of spectra of starburst regions in the low-redshift galaxies ESO 338-IG04 and Haro 11, obtained as part of the Science Verification Program of the X-Shooter spectrograph mounted on the Very Large Telescope in Paranal, Chile, operated by the European Southern Observatory consortium, in August 2009. These spectra had good seeing and extremely high SNR, allowing for a good resolution both spatially and kinematically (the high SNR allows for decomposition of the line shape into a number of components originating in different subsystems).

In the raw 2D spectra and rectified 2D science products, it is clearly visible that there is strong, and kinematically complex, line emission across a large fraction of the slit length. Since the SNR was good enough, the basic idea was therefore to extract and treat each pixel row as an individual spectrum, and

model its emission lines as the combination of a number of Gaussian emission peaks with the added constraint that the models must be consistent between adjacent rows[1], at least across the width of a seeing disk. Components behaving continuously over a spatial region could then be identified as originating from the same physical subsystem, which could then be analyzed individually.

Thanks to this, it was possible to identify an number of subsystems for each spectrum, and characterize each of them using the methods described in Sects. 2.5. One of the original ideas of the project was to attempt to map dust extinction to depth and create depth map of the subsystems; however, the results of this turned out to be ambiguous or just plain messy, possibly because of the very complex kinematics of the systems, which are all interacting or merging and therefore highly disrupted, or because the dust distribution is uneven and clumpy down to spatial scales smaller than the resolution; something the presence of known dust lanes in both knots of Haro 11 could suggest.

Data preparation and modelling/fitting work was quite extensive for this project. Raw data was reduced with the X-Shooter pipeline, except for the final extraction step. The spectra were taken in `nodding` mode, with two exposures offset along the slit axis but overlapping. The two exposures were then offset and combined into one 2D spectrum with a synthesized slit length almost 30% longer than the physical one.

To manage the modelling, fitting and generally high amount of bookkeeping required for a project of this kind, I wrote an interactive application which managed the fitting, navigation, interfaces with eh fitting software etc.

4.3 Paper IV and V

Even though star forming galaxies are expected to deliver the majority of the ionizing photons responsible for reionizing the Universe, starburst galaxies in the local Universe show very few Lyman Continuum leakers, and at very low escape fractions of only a few percent.

The galaxies Haro 11 and Tololo 1247-232 were the two first confirmed Lyman Continuum leakers (Bergvall et al., 2006; Leitet et al., 2011, 2013) both with quite uncertain and very faint signal in the ionizing continuum. **Paper IV** (Puschnig et al., submitted to MNRAS), is centered around HST-COS, far-UV spectroscopy of Tololo 1247, obtained for the purpose. The article's first author developed a modified version of the HST-COS data reduction pipeline,

[1]A constraint which in fact helped avoid one often-encountered problem in spectroscopic modelling: determining how many components should be included in the model without just beginning to fit the noise. Since the noise is random, it will not be spatially coherent and thus, such components are quite easily spotted in the 2D model.

optimizing the signal to noise in the Lyman Continuum. We analyzed the Si II absorption lines as described in sect. 2.3, and compared these results to the Lyα profile to constrain the neutral Hydrogen column density and compare these measurements to theoretical predictions stemming from either sparse, ionized gas model or a model of denser, neutral but perforated gas allowing for direct escape through select sight lines. The paper also utilizes auxiliary radio data in an attempt to derive a total mass of ionized, atomic and molecular gas and test relations between escape fraction and gas mass.

Paper V is a short paper containing a subset of the analysis of Tololo 1247 in Paper IV applied on Haro 11, with an apparent-optical-depth analysis of the UV Si II absorption line from a HST-COS spectrum, and comparison with its Lyα profile to probe neutral gas density and configuration, and again compare to the two model extremes of an optically thin and ionized or perforated, but optically thick and more neutral gas from Verhamme et al. (2015). The UV spectrum of Haro 11 is very similar to that of Tololo 1247, although the latter has somewhat lower neutral column density along the line of sight, and we reach similar conclusion in the two papers, although the gas masses for the two galaxies are quite different.

Sammanfattning

Aktivt stjärnbildande galaxer är en viktig och värdefull källa till kunskap om förhållanden i det unga, avlägsna universum. Med en hög frekvens av interaktioner och krockar, stark stjärnbildningsaktivitet, komplicerad kinematik och ofta rubbade eller helt oregelbundna former, är det en vanlig uppfattning bland astronomer att dessa galaxer är det närmaste vi kommer en lokal analog till galaxerna i universums barndom. De är därför mycket värdefulla som nyckel till att förstå vad vi ser när vi observerar unga galaxer vid hög rödförskjutning i det unga universum. Dessa unga galaxer i sin tur är viktiga nycklar till kosmologisk insikt om universums tidigaste epoker, t.ex. de första stjärnornas uppkomst, hur universums storskaliga struktur bildats, och det tidiga universums återjonisering.

Många av dessa tidiga, avlägsna galaxerna är primärt eller uteslutande synliga i våglängdsområdet runt den så kallade Lyman α (Lyα) linjen; våglängden motsvarande energin i övergången från första exciterade energinivån till grundnivån i en neutral väteatom. Lyα-strålning utsänds från från de centrala delarna av en galax och växelverkar starkt med neutrala vätemoln i och omkring galaxen. Ofta transporteras en Lyα-foton genom talrika växelverkningar lång bort från sin ursprungspunkt innan den antingen absorberas av stoftpartiklar eller slipper ut ur galaxen till den intergalaktiska rymden. Trots Lyα-linjens ursprungliga styrka absorberas den ofta totalt, eller sprids ut över stora projicerade arealer med relativt låg ytdensitet. Den ljusstyrka som observeras i Lyα är statistiskt nästan fullständigt frånkopplad från den ursprungliga styrkan och regleras i huvudsak av fysiska förhållanden i gasen, som strålningen passerar genom. För att kunna tolka observationer av Lyα vid hög rödförskjutning rätt är det därför viktigt att förstå, vilka processer som reglerar, och vilka förhållanden som tillåter, att strålningen slipper ut ur galaxen.

Unga, så kallade starburst-galaxer anses även vara den mest sannolika huvudorsaken till återjoniseringen av det unga universum. För att kunna göra detta måste de joniserande UV-fotonerna (i det så kallade Lyman Continuum), som produceras i de centrala starburst-regionerna av dessa galaxer, lyckas slippa igenom galaxens många och ofta tjocka vätemoln och ut ur galaxen. Precis som med Lyα, interagerar även dessa Lyman Continuum-fotoner med neutrala vätemoln, fast inte lika starkt som Lyα. Dock är det tillräckligt starkt för att astronomer, när detta projekt påbörjades, ba- ra skulle känna till två ga-

laxer som utstrålar mätbara mängder Lyman Continuum-strålning. Sedan dess har det hittats ett tiotals kandidater och bekräftade fall där Lyman Continuum-fotoner observerats från lokala galaxer, men fortfarande långt ifrån tillräckligt med joniserande strålning för att återjonisera det unga universum. Astronomer arbetar därför med att identifiera vilka egenskaper hos det interstellara mediet som reglerar Lyman Continuum-utstrålning, och hur dessa utvecklar sig med rödförskjutning över kosmologisk tid.

Denna avhandling består av projekt som, var på sitt sätt, syftar till att förbättra vår förståelse av dessa frågor. Det första projektet, the Lyman Alpha Reference Sample (LARS), har som målsättning att förstå vilka processer som reglerar Lyα-strålningstransport genom fördjupade studier av 14 lokala, stjärnbildande galaxer med en rad av kraftfulla teleskop och instrument. Mitt bidrag var spektroskopisk analys av de centrala stjärnbildande regionerna för att förstå dessa regioners fysiska egenskaper (Artikel I); och av neutrala vätemolnen genom vilka Lyα-strålningen måste transporteras för att nå fram till våra teleskop (Artikel II). I Artikel III företar vi ännu djupare, mer detaljerade spektroskopiska studier av de heta centrala, högt joniserade regionerna i två lokala, stjärnbildande galaxer. I Artikel IV och V flyttas fokus till att kombinera den tillgängliga informationen om Lyα och Lyman Continuum-strålning i de två första kända Lyman Continuum-utstrålande galaxerna för att förstå vilka konfigurationer av det interstellara mediet som kan föranleda utstrålning av joniserande fotoner och Lyα i den utformning det observeras.

Acknowledgements

Many people deserve thanks & praise for their role in helping me along to this point, but one more than anyone else: my wife **Christina Rivera-Thorsen**, without whose steady hand on the family logistics, this project would have been very difficult. To our kids **Eskil** and **Storm**, thank you for being patient with me even when at times I have been way too busy with work to play all the games with you. My parents **Karen Thorsen** and **Palle Juul Holm**, for inspiring me and encouraging me to do the things I liked and do them well, and my siblings, especially my little sisters **Bengerd Juul Thorsen** and **Petra Thorsen-Cheng** for being great siblings and aunts's and uncle'ses.

Professionally, above and before all I owe great thanks to my thesis advisors **Göran Östlin** and **Matthew Hayes** for giving me the chance to do this, and for their generosity in several aspects. Göran as my primary advisor for giving me the position in the first place, for great creative freedom on the way, and for support and patience when things were difficult. Matthew as my secondary advisor for not treating me as his secondary student, but always having time for answering questions, giving advise and suggestions and generally keeping in touch. Furthermore, I would like to thank my mentor, **Garrelt Mellema**, for keeping a keen eye on my well being in the daily, non-scientific matters.

An important part of my Ph.D. time has been my office mates. **Javier Blasco Herrera**, who was friendly and generous with laughs and rookie advise during the brief first time. Next, a big thank you to **Florent Duval** for the largest chunk of time in the middle, for lots of interesting scientific discussions and mutual help and advise, and for keeping me on my toes – for an ever so brief moment there, I fully believed in zombies. Finally, thanks to **Veronica Menacho** for bearing with me towards the end, when looming deadlines diverted my attention from more pedestrian matters like remembering to remove my leftover food from my desk.

I have enjoyed the company of many people in the department, especially fellow Ph.D. students. My "Ph.D. brothers" **Kai-Yan Lee** and **Gianni Cataldi**, and I guess **Andreas Sandberg** also somehow fits in this category – the latter has also been a great help and collaborar in teaching and a valuable source of little pieces of useful information that would have been hard to find elsewhere. I also think **Saghar Asadi**, **Egil Möller** for many of the same things as ap-

ply to Saghar **Hiva Pazhira** and **Katia Migotto** deserve special mention, for good company at and outside of work, and for taking such a great interest in our kids, and Egil for help with the Swedish abstract for this thesis. To **Illa Rivero-Llosada** for parties and playdates with the kids. **Alessandro Razza**, **Anil Gumus** for delicious food and moving help. To **Francesco Taddia** for many good talks. And all the others that I have forgotten at this moment – my apologies.

I have worked with interesting fellow students and met new friends in conferences and summer/winter schools. I want to thank **Livia Vallini** and **Eskil Varenius** for being perhaps the best group I have worked in, and definitely the only one where I was ever first in alphabetic order. To **Sinziana Paduroiu** for rewarding conversations about life, the Universe and the perils of thesis writing. To **Alex** and **Leah hagen** for generously extending their friendship my way. A special thanks is due to **Beatriz Villarroel**, for always being generous with her time and expertise.

A portion of my time has been spent abroad, especially in the Twin Cities, Minnesota. Here, I wish to thank especially **John M. Cannon** from the LARS collaboration, for generously hosting me and allowing me to collaborate and take part in the academic life on Macalester College. **Claudia Scarlata** at the U of M, for taking an interest in my work and progress and taking the time to provide me advise and feedback where she had no sort of obligation, formal or informal, to do so. To **Elise Larson** and **Stephen Pardy** for patiently guiding me through the treacherous jungle that is CASA, and to **Michael Rutkowski** for help, scientific discussions, and baseball. And my in-laws, **Cheryl** and **Refugio Rivera** for their great hospitality.

I also feel grateful to a great many people in LARS and the broader astronomical community for help, support, rewarding scientific discourse and encouragement at different stages of this project – the list includes but is not limited to **Erik Zackrisson** - for knowing how to make science fun while keepinng it serious - and **Jens Melinder**, **Angela Adamo**, **Emily Freeland**, **Ivana Orlitóva**, **Anne Verhamme**, **Miguel Más-Hesse**, **Daniel kunth**, **Peter Laursen** and the rest of LARS; to **Mark Dijkstra**,**Signe Riemer-Sørensen**, and the group in Oslo; **Sangeeta Malhotra**, **James Rhoads**, **Johan P. U. Fynbo**, **Lise Christensen**, **Marianne Vestergård**, and most likely someone I have forgotten.

Outside of academia, I first of all want to thank **Sune Hvidtfeldt Håkansson** for his heroic contribution to our move, and to friends back in Denmark who have been nice and hopsitable – besides the already mentioned, that would be **Stine Kjær** and **Tali Jensen**, and **Kasper Risager** and **Sine Sambach**, and to the old new year's crew for keeping the line alive. Next, I want to thank old and new Swedish friends for making the time here much more fun: espe-

cially **Micke Hanås**, **Chrille Eriksson**, **Jimmie Lazenby**, **Sara Hale**, **Malin Svantesson**, **Anna Palmqvist**, **Johannes Penton**, **Otto Rimfors** and the rest of the Bagis gang of yore, for party and hangout and conversation and moving help. To **Johan Henriksson** and **André Hansen** for help and beers, and to **Vesa Nurminen** and family for nice playground dates.

References

T. F. Adams. The Escape of Resonance-Line Radiation from Extremely Opaque Media. ApJ, 174:439, June 1972. doi: 10.1086/151503. 34

M. Ajiki, Y. Taniguchi, S. S. Fujita, Y. Shioya, T. Nagao, T. Murayama, S. Yamada, K. Umeda, and Y. Komiyama. A Subaru Search for Lyα Emitters at Redshift 5.7. AJ, 126:2091–2107, November 2003. doi: 10.1086/378481. 15

D. Alloin, S. Collin-Souffrin, M. Joly, and L. Vigroux. Nitrogen and oxygen abundances in galaxies. A&A, 78:200–216, September 1979. 63

Hakim Atek, Daniel Kunth, Daniel Schaerer, J. Miguel Mas-Hesse, Matthew Hayes, Göran Östlin, and Jean-Paul Kneib. Influence of physical galaxy properties on Ly α escape in star-forming galaxies. *Astronomy & Astrophysics*, 561:A89, January 2014. ISSN 0004-6361. doi: 10.1051/0004-6361/201321519. URL `http://adsabs.harvard.edu/abs/2014A&A...561A..89A`. 32

E. Baron and S. D. M. White. The appearance of primeval galaxies. ApJ, 322:585–596, November 1987. doi: 10.1086/165754. 22, 23, 24

R. H. Becker, X. Fan, R. L. White, M. A. Strauss, V. K. Narayanan, R. H. Lupton, J. E. Gunn, J. Annis, N. A. Bahcall, J. Brinkmann, A. J. Connolly, I. Csabai, P. C. Czarapata, M. Doi, T. M. Heckman, G. S. Hennessy, Ž. Ivezić, G. R. Knapp, D. Q. Lamb, T. A. McKay, J. A. Munn, T. Nash, R. Nichol, J. R. Pier, G. T. Richards, D. P. Schneider, C. Stoughton, A. S. Szalay, A. R. Thakar, and D. G. York. Evidence for Reionization at z˜6: Detection of a Gunn-Peterson Trough in a z=6.28 Quasar. AJ, 122:2850–2857, December 2001. doi: 10.1086/324231. 38, 39

N. Bergvall, E. Zackrisson, B.-G. Andersson, D. Arnberg, J. Masegosa, and G. Östlin. First detection of Lyman continuum escape from a local starburst galaxy. I. Observations of the luminous blue compact galaxy Haro 11 with the Far Ultraviolet Spectroscopic Explorer (FUSE). A&A, 448:513–524, March 2006. doi: 10.1051/0004-6361:20053788. 72

Y. Birnboim and A. Dekel. Virial shocks in galactic haloes? MNRAS, 345:349–364, October 2003. doi: 10.1046/j.1365-8711.2003.06955.x. 18

N. A. Bond, E. Gawiser, C. Gronwall, R. Ciardullo, M. Altmann, and K. Schawinski. Sizes of LYα-emitting Galaxies and Their Rest-frame Ultraviolet Components at z = 3.1. ApJ, 705:639–649, November 2009. doi: 10.1088/0004-637X/705/1/639. 24, 28

R. J. Bouwens, G. D. Illingworth, M. Franx, and H. Ford. UV Luminosity Functions at z˜4, 5, and 6 from the Hubble Ultra Deep Field and Other Deep Hubble Space Telescope ACS Fields: Evolution and Star Formation History. ApJ, 670:928–958, December 2007. doi: 10.1086/521811. 26

R. J. Bouwens, G. D. Illingworth, M. Franx, and H. Ford. z ˜ 7-10 Galaxies in the HUDF and GOODS Fields: UV Luminosity Functions. ApJ, 686:230–250, October 2008. doi: 10.1086/590103. 26

S. Charlot and S. M. Fall. Lyman-Alpha Emission from Galaxies. ApJ, 415:580, October 1993. doi: 10.1086/173187. 19, 22, 24, 26, 27, 31

L. L. Cowie and E. M. Hu. High-z Lyalpha Emitters. I. A Blank-Field Search for Objects near Redshift Z = 3.4 in and around the Hubble Deep Field and the Hawaii Deep Field SSA 22. AJ, 115:1319–1328, April 1998. doi: 10.1086/300309. 15, 27

L. L. Cowie, A. J. Barger, and E. M. Hu. Low-Redshift Lyα Selected Galaxies from GALEX Spectroscopy: A Comparison with Both UV-Continuum Selected Galaxies and High-Redshift Lyα Emitters. ApJ, 711: 928–958, March 2010. doi: 10.1088/0004-637X/711/2/928. 28, 35

L. L. Cowie, A. J. Barger, and E. M. Hu. Lyα Emitting Galaxies as Early Stages in Galaxy Formation. ApJ, 738:136, September 2011. doi: 10.1088/0004-637X/738/2/136. 28

P. Dayal, A. Ferrara, and A. Saro. The cool side of Lyman alpha emitters. MNRAS, 402:1449–1457, March 2010. doi: 10.1111/j.1365-2966.2009.15995.x. 18

G. Denicoló, R. Terlevich, and E. Terlevich. New light on the search for low-metallicity galaxies - I. The N2 calibrator. MNRAS, 330:69–74, February 2002. doi: 10.1046/j.1365-8711.2002.05041.x. 62

M. Dijkstra and A. Loeb. Lyα blobs as an observational signature of cold accretion streams into galaxies. MNRAS, 400:1109–1120, December 2009. doi: 10.1111/j.1365-2966.2009.15533.x. 18

M. Dijkstra, Z. Haiman, and M. Spaans. Lyα Radiation from Collapsing Protogalaxies. I. Characteristics of the Emergent Spectrum. ApJ, 649:14–36, September 2006. doi: 10.1086/506243. 28

M. Dijkstra, J. S. B. Wyithe, and Z. Haiman. Luminosity functions of Lyα emitting galaxies and cosmic reionization of hydrogen. MNRAS, 379:253–259, July 2007. doi: 10.1111/j.1365-2966.2007.11936.x. 15

Mark Dijkstra. Lyman Alpha Emitting Galaxies as a Probe of Reionization. page 27, June 2014. URL `http://arxiv.org/abs/1406.7292`. 16, 18, 42

B. T. Draine. *Physics of the Interstellar and Intergalactic Medium*. 2011. 60, 61

S.R. Drayson. Rapid computation of the Voigt profile. *Journal of Quantitative Spectroscopy and Radiative Transfer*, 16(7):611–614, July 1976. ISSN 00224073. doi: 10.1016/0022-4073(76)90029-7. URL `http://linkinghub.elsevier.com/retrieve/pii/0022407376900297`. 47

F. Duval, D. Schaerer, G. Östlin, and P. Laursen. Lyman α line and continuum radiative transfer in a clumpy interstellar medium. A&A, 562:A52, February 2014. doi: 10.1051/0004-6361/201220455. 32, 34, 35

H. C. Ferguson, M. Dickinson, M. Giavalisco, C. Kretchmer, S. Ravindranath, R. Idzi, E. Taylor, C. J. Conselice, S. M. Fall, J. P. Gardner, M. Livio, P. Madau, L. A. Moustakas, C. M. Papovich, R. S. Somerville, H. Spinrad, and D. Stern. The Size Evolution of High-Redshift Galaxies. ApJ, 600:L107–L110, January 2004. doi: 10.1086/378578. 24

S. L. Finkelstein, J. E. Rhoads, S. Malhotra, N. Pirzkal, and J. Wang. The Ages and Masses of Lyα Galaxies at z ˜ 4.5. ApJ, 660:1023–1029, May 2007. doi: 10.1086/513462. 28

J. U. Fynbo, P. Möller, and B. Thomsen. Probing the faint end of the Galaxy luminosity function at z= 3 with Lyalpha emission. A&A, 374:443–453, August 2001. doi: 10.1051/0004-6361:20010739. 29

E. Gawiser, P. G. van Dokkum, C. Gronwall, R. Ciardullo, G. A. Blanc, F. J. Castander, J. Feldmeier, H. Francke, M. Franx, L. Haberzettl, D. Herrera, T. Hickey, L. Infante, P. Lira, J. Maza, R. Quadri, A. Richardson, K. Schawinski, M. Schirmer, E. N. Taylor, E. Treister, C. M. Urry, and S. N. Virani. The Physical Nature of Lyα-emitting Galaxies at z=3.1. ApJ, 642:L13–L16, May 2006. doi: 10.1086/504467. 28

E. Gawiser, H. Francke, K. Lai, K. Schawinski, C. Gronwall, R. Ciardullo, R. Quadri, A. Orsi, L. F. Barrientos, G. A. Blanc, G. Fazio, J. J. Feldmeier, J.-s. Huang, L. Infante, P. Lira, N. Padilla, E. N. Taylor, E. Treister, C. M. Urry, P. G. van Dokkum, and S. N. Virani. Lyα-Emitting Galaxies at z = 3.1: L* Progenitors Experiencing Rapid Star Formation. ApJ, 671:278–284, December 2007. doi: 10.1086/522955. 28

M. Giavalisco, C. C. Steidel, and F. D. Macchetto. Hubble Space Telescope Imaging of Star-forming Galaxies at Redshifts Z 3. ApJ, 470:189, October 1996. doi: 10.1086/177859. 15, 22, 31

M. Gronke and M. Dijkstra. Directional Lyα equivalent boosting - I. Spherically symmetric distributions of clumps. MNRAS, 444:1095–1103, October 2014. doi: 10.1093/mnras/stu1513. 35

C. Gronwall, R. Ciardullo, T. Hickey, E. Gawiser, J. J. Feldmeier, P. G. van Dokkum, C. M. Urry, D. Herrera, B. D. Lehmer, L. Infante, A. Orsi, D. Marchesini, G. A. Blanc, H. Francke, P. Lira, and E. Treister. Lyα Emission-Line Galaxies at z = 3.1 in the Extended Chandra Deep Field-South. ApJ, 667:79–91, September 2007. doi: 10.1086/520324. 23, 24, 28

L. Guaita, E. Gawiser, N. Padilla, H. Francke, N. A. Bond, C. Gronwall, R. Ciardullo, J. J. Feldmeier, S. Sinawa, G. A. Blanc, and S. Virani. Lyα-emitting Galaxies at z = 2.1 in ECDF-S: Building Blocks of Typical Present-day Galaxies? ApJ, 714:255–269, May 2010. doi: 10.1088/0004-637X/714/1/255. 43

L. Guaita, J. Melinder, M. Hayes, G. Östlin, J. E. Gonzalez, G. Micheva, A. Adamo, J. M. Mas-Hesse, A. Sandberg, H. Otí-Floranes, D. Schaerer, A. Verhamme, E. Freeland, I. Orlitová, P. Laursen, J. M. Cannon, F. Duval, T. Rivera-Thorsen, E. C. Herenz, D. Kunth, H. Atek, J. Puschnig, P. Gruyters, and S. A. Pardy. The Lyman alpha reference sample. IV. Morphology at low and high redshift. A&A, 576: A51, April 2015. doi: 10.1051/0004-6361/201425053. 66

J. E. Gunn and B. A. Peterson. On the Density of Neutral Hydrogen in Intergalactic Space. ApJ, 142: 1633–1641, November 1965. doi: 10.1086/148444. 38

A. Hagen, R. Ciardullo, C. Gronwall, V. Acquaviva, J. Bridge, G. R. Zeimann, G. A. Blanc, N. A. Bond, S. L. Finkelstein, M. Song, E. Gawiser, D. B. Fox, H. Gebhardt, A. I. Malz, D. P. Schneider, N. Drory, K. Gebhardt, and G. J. Hill. Spectral Energy Distribution Fitting of HETDEX Pilot Survey Lyα Emitters in COSMOS and GOODS-N. ApJ, 786:59, May 2014. doi: 10.1088/0004-637X/786/1/59. 28

M. Hansen and S. P. Oh. Lyman α radiative transfer in a multiphase medium. MNRAS, 367:979–1002, April 2006. doi: 10.1111/j.1365-2966.2005.09870.x. 34

G. Haro. Preliminary Note on Blue Galaxies with emission lines (*Spanish Title: Nota preliminar sobre Galaxias Azules con Líneas de Emisión*). *Boletin de los Observatorios Tonantzintla y Tacubaya*, 2: 8–18, June 1956. 20

L. W. Hartmann, J. P. Huchra, and M. J. Geller. How to find galaxies at high redshift. ApJ, 287:487–491, December 1984. doi: 10.1086/162707. 15, 21, 31

T. Hashimoto, M. Ouchi, K. Shimasaku, Y. Ono, K. Nakajima, M. Rauch, J. Lee, and S. Okamura. Gas Motion Study of Lyα Emitters at z ˜ 2 Using FUV and Optical Spectral Lines. ApJ, 765:70, March 2013. doi: 10.1088/0004-637X/765/1/70. 41

M. Hayes. *PASA*, WhoKnows 2015. 22, 26, 27, 28

M. Hayes, G. Östlin, J. M. Mas-Hesse, D. Kunth, C. Leitherer, and A. Petrosian. HST/ACS Lyman α imaging of the nearby starburst ESO 338-IG04. A&A, 438:71–85, July 2005. doi: 10.1051/0004-6361: 20052702. 29

M. Hayes, G. Östlin, J. M. Mas-Hesse, and D. Kunth. Continuum Subtracting Lyman-Alpha Images: Low-Redshift Studies Using the Solar Blind Channel of HST/ACS. AJ, 138:911–922, September 2009. doi: 10.1088/0004-6256/138/3/911. 30

M. Hayes, D. Schaerer, G. Östlin, J. M. Mas-Hesse, H. Atek, and D. Kunth. On the Redshift Evolution of the Lyα Escape Fraction and the Dust Content of Galaxies. ApJ, 730:8, March 2011. doi: 10.1088/ 0004-637X/730/1/8. 28, 40

M. Hayes, G. Östlin, D. Schaerer, A. Verhamme, J. M. Mas-Hesse, A. Adamo, H. Atek, J. M. Cannon, F. Duval, L. Guaita, E. C. Herenz, D. Kunth, P. Laursen, J. Melinder, I. Orlitová, H. Otí-Floranes, and A. Sandberg. The Lyman Alpha Reference Sample: Extended Lyman Alpha Halos Produced at Low Dust Content. ApJ, 765:L27, March 2013. doi: 10.1088/2041-8205/765/2/L27. 65

M. Hayes, G. Östlin, F. Duval, A. Sandberg, L. Guaita, J. Melinder, A. Adamo, D. Schaerer, A. Verhamme, I. Orlitová, J. M. Mas-Hesse, J. M. Cannon, H. Atek, D. Kunth, P. Laursen, H. Otí-Floranes, S. Pardy, T. Rivera-Thorsen, and E. C. Herenz. The Lyman Alpha Reference Sample. II. Hubble Space Telescope Imaging Results, Integrated Properties, and Trends. ApJ, 782:6, February 2014. doi: 10.1088/0004-637X/782/1/6. xi, 66, 67, 69, 70

T. M. Heckman, S. Borthakur, R. Overzier, G. Kauffmann, A. Basu-Zych, C. Leitherer, K. Sembach, D. C. Martin, R. M. Rich, D. Schiminovich, and M. Seibert. Extreme Feedback and the Epoch of Reionization: Clues in the Local Universe. ApJ, 730:5, March 2011. doi: 10.1088/0004-637X/730/1/5. 43

E. C. Herenz, P. Gruyters, I. Orlitova, M. Hayes, G. Östlin, J. M. Cannon, M. M. Roth, A. Bik, S. Pardy, H. Otí-Floranes, J. M. Mas-Hesse, A. Adamo, H. Atek, F. Duval, L. Guaita, D. Kunth, P. Laursen, J. Melinder, J. Puschnig, T. E. Rivera-Thorsen, D. Schaerer, and A. Verhamme. The Lyman alpha reference sample. VII. Spatially resolved Hα kinematics. A&A, 587:A78, March 2016. doi: 10.1051/0004-6361/201527373. 67

G. Hinshaw, D. Larson, E. Komatsu, D. N. Spergel, C. L. Bennett, J. Dunkley, M. R. Nolta, M. Halpern, R. S. Hill, N. Odegard, L. Page, K. M. Smith, J. L. Weiland, B. Gold, N. Jarosik, A. Kogut, M. Limon, S. S. Meyer, G. S. Tucker, E. Wollack, and E. L. Wright. Nine-year Wilkinson Microwave Anisotropy Probe (WMAP) Observations: Cosmological Parameter Results. ApJS, 208:19, October 2013. doi: 10.1088/0067-0049/208/2/19. 39

E. M. Hu, L. L. Cowie, and R. G. McMahon. The Density of Lyα Emitters at Very High Redshift. ApJ, 502:L99–L103, August 1998. doi: 10.1086/311506. 15, 27

Y. I. Izotov, G. Stasińska, G. Meynet, N. G. Guseva, and T. X. Thuan. The chemical composition of metal-poor emission-line galaxies in the Data Release 3 of the Sloan Digital Sky Survey. A&A, 448:955–970, March 2006. doi: 10.1051/0004-6361:20053763. 61

A. E. Jaskot and M. S. Oey. The Origin and Optical Depth of Ionizing Radiation in the "Green Pea" Galaxies. ApJ, 766:91, April 2013. doi: 10.1088/0004-637X/766/2/91. 43

A. E. Jaskot and M. S. Oey. Linking Lyα and Low-ionization Transitions at Low Optical Depth. ApJ, 791: L19, August 2014. doi: 10.1088/2041-8205/791/2/L19. 33

H. Jensen, P. Laursen, G. Mellema, I. T. Iliev, J. Sommer-Larsen, and P. R. Shapiro. On the use of Lyα emitters as probes of reionization. MNRAS, 428:1366–1381, January 2013. doi: 10.1093/mnras/sts116. 15, 40, 42

T. A. Jones, R. S. Ellis, M. A. Schenker, and D. P. Stark. Keck Spectroscopy of Gravitationally Lensed z ˜= 4 Galaxies: Improved Constraints on the Escape Fraction of Ionizing Photons. ApJ, 779:52, December 2013. doi: 10.1088/0004-637X/779/1/52. 27, 48, 52, 53, 54

N. Kashikawa, T. Nagao, J. Toshikawa, Y. Ishizaki, E. Egami, M. Hayashi, C. Ly, M. A. Malkan, Y. Matsuda, K. Shimasaku, M. Iye, K. Ota, T. Shibuya, L. Jiang, Y. Taniguchi, and Y. Shioya. A Lyα Emitter with an Extremely Large Rest-frame Equivalent Width of ˜900 Å at z = 6.5: A Candidate Population III-dominated Galaxy? ApJ, 761:85, December 2012. doi: 10.1088/0004-637X/761/2/85. 18

R. C. Kennicutt, Jr., F. Bresolin, and D. R. Garnett. The Composition Gradient in M101 Revisited. II. Electron Temperatures and Implications for the Nebular Abundance Scale. ApJ, 591:801–820, July 2003. doi: 10.1086/375398. 62

L. J. Kewley and M. A. Dopita. Using Strong Lines to Estimate Abundances in Extragalactic H II Regions and Starburst Galaxies. ApJS, 142:35–52, September 2002. doi: 10.1086/341326. 62

K. Kovač, R. S. Somerville, J. E. Rhoads, S. Malhotra, and J. Wang. Clustering of Lyα Emitters at z ˜ 4.5. ApJ, 668:15–22, October 2007. doi: 10.1086/520668. 43

R.-P. Kudritzki, R. H. Méndez, J. J. Feldmeier, R. Ciardullo, G. H. Jacoby, K. C. Freeman, M. Arnaboldi, M. Capaccioli, O. Gerhard, and H. C. Ford. Discovery of Nine Lyα Emitters at Redshift z˜3.1 Using Narrowband Imaging and VLT Spectroscopy. ApJ, 536:19–30, June 2000. doi: 10.1086/308925. 15

D. Kunth, J. Lequeux, W. L. W. Sargent, and F. Viallefond. Is there primordial gas in IZw 18? A&A, 282: 709–716, February 1994. 26, 32

Daniel Kunth, J.˜M. Mas-Hesse, E Terlevich, R Terlevich, J Lequeux, and S.˜M. Michael Fall. HST study of Lyman-alpha emission in star-forming galaxies : the effect of neutral gas flows. *Astronomy and Astrophysics*, 20:11–20, June 1998. 27, 33, 48, 71

J. H. Lacy, M. Malkan, E. E. Becklin, B. T. Soifer, G. Neugebauer, K. Matthews, C.-C. Wu, A. Boggess, and T. R. Gull. Infrared, optical, and ultraviolet observations of hydrogen line emission from Seyfert galaxies. ApJ, 256:75–82, May 1982. doi: 10.1086/159884. 15, 21

P. Laursen and J. Sommer-Larsen. Lyα Resonant Scattering in Young Galaxies: Predictions from Cosmological Simulations. ApJ, 657:L69–L72, March 2007. doi: 10.1086/513191. 34, 35

P. Laursen, A. O. Razoumov, and J. Sommer-Larsen. Lyα Radiative Transfer in Cosmological Simulations Using Adaptive Mesh Refinement. ApJ, 696:853–869, May 2009a. doi: 10.1088/0004-637X/696/1/853. 29, 33, 34, 35

P. Laursen, J. Sommer-Larsen, and A. C. Andersen. Lyα Radiative Transfer with Dust: Escape Fractions from Simulated High-Redshift Galaxies. ApJ, 704:1640–1656, October 2009b. doi: 10.1088/0004-637X/704/2/1640. 35, 66

P. Laursen, J. Sommer-Larsen, and A. O. Razoumov. Intergalactic Transmission and Its Impact on the Lyα Line. ApJ, 728:52, February 2011. doi: 10.1088/0004-637X/728/1/52. 41

P. Laursen, F. Duval, and G. Östlin. On the (Non-)Enhancement of the Lyα Equivalent Width by a Multiphase Interstellar Medium. ApJ, 766:124, April 2013. doi: 10.1088/0004-637X/766/2/124. 18, 32, 34, 35

K.-G. Lee, J. F. Hennawi, C. Stark, J. X. Prochaska, M. White, D. J. Schlegel, A.-C. Eilers, A. Arinyo-i-Prats, N. Suzuki, R. A. C. Croft, K. I. Caputi, P. Cassata, O. Ilbert, B. Garilli, A. M. Koekemoer, V. Le Brun, O. Le Fèvre, D. Maccagni, P. Nugent, Y. Taniguchi, L. A. M. Tasca, L. Tresse, G. Zamorani, and E. Zucca. Lyα Forest Tomography from Background Galaxies: The First Megaparsec-resolution Large-scale Structure Map at z $>$ 2. ApJ, 795:L12, November 2014. doi: 10.1088/2041-8205/795/1/L12. 38

E. Leitet, N. Bergvall, N. Piskunov, and B.-G. Andersson. Analyzing low signal-to-noise FUSE spectra. Confirmation of Lyman continuum escape from Haro 11. A&A, 532:A107, August 2011. doi: 10.1051/0004-6361/201015654. 72

E. Leitet, N. Bergvall, M. Hayes, S. Linné, and E. Zackrisson. Escape of Lyman continuum radiation from local galaxies. Detection of leakage from the young starburst Tol 1247-232. A&A, 553:A106, May 2013. doi: 10.1051/0004-6361/201118370. 72

J. Lequeux, D. Kunth, J. M. Mas-Hesse, and W. L. W. Sargent. Galactic wind and Lyman α emission in the blue compact galaxy Haro 2 = MKN 33. A&A, 301:18, September 1995. 26, 33

V. Luridiana, C. Morisset, and R. A. Shaw. PyNeb: a new tool for analyzing emission lines. I. Code description and validation of results. A&A, 573:A42, January 2015. doi: 10.1051/0004-6361/201323152. 56, 61

C. Ly, M. A. Malkan, T. Treu, J.-H. Woo, T. Currie, M. Hayashi, N. Kashikawa, K. Motohara, K. Shimasaku, and M. Yoshida. Lyman Break Galaxies at z $\approx$ 1.8-2.8: GALEX/NUV Imaging of the Subaru Deep Field. ApJ, 697:1410–1432, June 2009. doi: 10.1088/0004-637X/697/2/1410. 26

C. Ly, M. A. Malkan, M. Hayashi, K. Motohara, N. Kashikawa, K. Shimasaku, T. Nagao, and C. Grady. A Census of Star-forming Galaxies at z = 1-3 in the Subaru Deep Field. ApJ, 735:91, July 2011. doi: 10.1088/0004-637X/735/2/91. 26

P. Madau, H. C. Ferguson, M. E. Dickinson, M. Giavalisco, C. C. Steidel, and A. Fruchter. High-redshift galaxies in the Hubble Deep Field: colour selection and star formation history to z˜4. MNRAS, 283: 1388–1404, December 1996. 26

S. Malhotra and J. E. Rhoads. Large Equivalent Width Lyα line Emission at z=4.5: Young Galaxies in a Young Universe? ApJ, 565:L71–L74, February 2002. doi: 10.1086/338980. 18

S. Malhotra and J. E. Rhoads. Luminosity Functions of Lyα Emitters at Redshifts z=6.5 and z=5.7: Evidence against Reionization at z=6.5. ApJ, 617:L5–L8, December 2004. doi: 10.1086/427182. 15

S. Malhotra, J. E. Rhoads, S. L. Finkelstein, N. Hathi, K. Nilsson, E. McLinden, and N. Pirzkal. Sizing up Lyα and Lyman Break Galaxies. ApJ, 750:L36, May 2012. doi: 10.1088/2041-8205/750/2/L36. 24, 28

R. A. Marino, F. F. Rosales-Ortega, S. F. Sánchez, A. Gil de Paz, J. Vílchez, D. Miralles-Caballero, C. Kehrig, E. Pérez-Montero, V. Stanishev, J. Iglesias-Páramo, A. I. Díaz, A. Castillo-Morales, R. Kennicutt, A. R. López-Sánchez, L. Galbany, R. García-Benito, D. Mast, J. Mendez-Abreu, A. Monreal-Ibero, B. Husemann, C. J. Walcher, B. García-Lorenzo, J. Masegosa, A. Del Olmo Orozco, A. M. Mourão, B. Ziegler, M. Mollá, P. Papaderos, P. Sánchez-Blázquez, R. M. González Delgado, J. Falcón-Barroso, M. M. Roth, G. van de Ven, and Califa Team. The O3N2 and N2 abundance indicators revisited: improved calibrations based on CALIFA and T_e-based literature data. A&A, 559:A114, November 2013. doi: 10.1051/0004-6361/201321956. 62, 63

J. M. Mas-Hesse, D. Kunth, G. Tenorio-Tagle, C. Leitherer, R. J. Terlevich, and E. Terlevich. Lyα Emission in Starbursts: Implications for Galaxies at High Redshift. ApJ, 598:858–877, December 2003. doi: 10.1086/379116. 33, 71

S. S. McGaugh. H II region abundances - Model oxygen line ratios. ApJ, 380:140–150, October 1991. doi: 10.1086/170569. 62

D. L. Meier. The Optical Appearance of Model Primeval Galaxies. ApJ, 207:343–350, July 1976. doi: 10.1086/154500. 19, 21

D. L. Meier and R. Terlevich. Extragalactic H II regions in the UV - Implications for primeval galaxies. ApJ, 246:L109–L113, June 1981. doi: 10.1086/183565. 19, 21, 26, 31

P. Moller and S. J. Warren. HST images of a galaxy group at z=2.81, and the sizes of damped Lyalpha galaxies. MNRAS, 299:661–671, September 1998. doi: 10.1046/j.1365-8711.1998.01749.x. 29

D. A. Neufeld. The transfer of resonance-line radiation in static astrophysical media. ApJ, 350:216–241, February 1990. doi: 10.1086/168375. 31, 32, 33, 34

D.˜A. Neufeld. The escape of Lyman-alpha radiation from a multiphase interstellar medium. *apjl*, 370: L85–L88, April 1991. doi: 10.1086/185983. 32, 34

P. A. Oesch, R. J. Bouwens, G. D. Illingworth, I. Labbé, M. Franx, P. G. van Dokkum, M. Trenti, M. Stiavelli, V. Gonzalez, and D. Magee. Probing the Dawn of Galaxies at z ˜ 9-12: New Constraints from HUDF12/XDF and CANDELS data. ApJ, 773:75, August 2013. doi: 10.1088/0004-637X/773/1/75. 26

P. A. Oesch, G. Brammer, P. G. van Dokkum, G. D. Illingworth, R. J. Bouwens, I. Labbé, M. Franx, I. Momcheva, M. L. N. Ashby, G. G. Fazio, V. Gonzalez, B. Holden, D. Magee, R. E. Skelton, R. Smit, L. R. Spitler, M. Trenti, and S. P. Willner. A Remarkably Luminous Galaxy at z=11.1 Measured with Hubble Space Telescope Grism Spectroscopy. ApJ, 819:129, March 2016. doi: 10.3847/0004-637X/819/2/129. 27

A. Orsi, C. G. Lacey, C. M. Baugh, and L. Infante. The clustering of Lyα emitters in a ΛCDM Universe. MNRAS, 391:1589–1604, December 2008. doi: 10.1111/j.1365-2966.2008.14010.x. 15

D. E. Osterbrock. The Escape of Resonance-Line Radiation from an Optically Thick Nebula. ApJ, 135: 195, January 1962. doi: 10.1086/147258. 31, 34

D. E. Osterbrock and G. J. Ferland. *Astrophysics of gaseous nebulae and active galactic nuclei*. 2006. 55, 56, 57, 58, 59

G. Östlin, M. Hayes, D. Kunth, J. M. Mas-Hesse, C. Leitherer, A. Petrosian, and H. Atek. The Lyman Alpha Morphology of Local Starburst Galaxies: Release of Calibrated Images. AJ, 138:923–940, September 2009. doi: 10.1088/0004-6256/138/3/923. 30

G. Östlin, M. Hayes, F. Duval, A. Sandberg, L. Guaita, J. Melinder, A. Adamo, D. Schaerer, A. Verhamme, I. Orlitová, J. M. Mas-Hesse, J. M. Cannon, H. Atek, D. Kunth, P. Laursen, H. Otí-Floranes, S. Pardy, T. Rivera-Thorsen, and E. C. Herenz. The Lyman Alpha Reference Sample. I. CORRECT INFO NEEDED ABOUT THIS PAPER. ApJ, 2014. 70

M. Ouchi, K. Shimasaku, S. Okamura, H. Furusawa, N. Kashikawa, K. Ota, M. Doi, M. Hamabe, M. Kimura, Y. Komiyama, M. Miyazaki, S. Miyazaki, F. Nakata, M. Sekiguchi, M. Yagi, and N. Yasuda. Subaru Deep Survey. V. A Census of Lyman Break Galaxies at z˜=4 and 5 in the Subaru Deep Fields: Photometric Properties. ApJ, 611:660–684, August 2004. doi: 10.1086/422207. 43

M. Ouchi, K. Shimasaku, M. Akiyama, K. Sekiguchi, H. Furusawa, S. Okamura, N. Kashikawa, M. Iye, T. Kodama, T. Saito, T. Sasaki, C. Simpson, T. Takata, T. Yamada, H. Yamanoi, M. Yoshida, and M. Yoshida. The Discovery of Primeval Large-Scale Structures with Forming Clusters at Redshift 6. ApJ, 620:L1–L4, February 2005. doi: 10.1086/428499. 15

M. Ouchi, K. Shimasaku, M. Akiyama, C. Simpson, T. Saito, Y. Ueda, H. Furusawa, K. Sekiguchi, T. Yamada, T. Kodama, N. Kashikawa, S. Okamura, M. Iye, T. Takata, M. Yoshida, and M. Yoshida. The Subaru/XMM-Newton Deep Survey (SXDS). IV. Evolution of Lyα Emitters from z=3.1 to 5.7 in the 1 deg^2 Field: Luminosity Functions and AGN. ApJS, 176:301–330, June 2008. doi: 10.1086/527673. 15, 28, 40

M. Ouchi, K. Shimasaku, H. Furusawa, T. Saito, M. Yoshida, M. Akiyama, Y. Ono, T. Yamada, K. Ota, N. Kashikawa, M. Iye, T. Kodama, S. Okamura, C. Simpson, and M. Yoshida. Statistics of 207 Lyα Emitters at a Redshift Near 7: Constraints on Reionization and Galaxy Formation Models. ApJ, 723: 869–894, November 2010. doi: 10.1088/0004-637X/723/1/869. 28, 40

B. E. J. Pagel, M. G. Edmunds, D. E. Blackwell, M. S. Chun, and G. Smith. On the composition of H II regions in southern galaxies. I - NGC 300 and 1365. MNRAS, 189:95–113, October 1979. doi: 10.1093/mnras/189.1.95. 62

S. A. Pardy, J. M. Cannon, G. Östlin, M. Hayes, T. Rivera-Thorsen, A. Sandberg, A. Adamo, E. Freeland, E. C. Herenz, L. Guaita, D. Kunth, P. Laursen, J. M. Mas-Hesse, J. Melinder, I. Orlitová, H. Otí-Floranes, J. Puschnig, D. Schaerer, and A. Verhamme. The Lyman Alpha Reference Sample. III. Properties of the Neutral ISM from GBT and VLA Observations. ApJ, 794:101, October 2014. doi: 10.1088/0004-637X/794/2/101. 33, 66

R. B. Partridge and P. J. E. Peebles. Are Young Galaxies Visible? *The Astrophysical Journal*, 147:868, March 1967. ISSN 0004-637X. doi: 10.1086/149079. URL `http://adsabs.harvard.edu/doi/10.1086/149079`. 17, 19, 21, 22

L. Pentericci, A. Grazian, A. Fontana, M. Castellano, E. Giallongo, S. Salimbeni, and P. Santini. The physical properties of Lyα emitting galaxies: not just primeval galaxies? A&A, 494:553–561, February 2009. doi: 10.1051/0004-6361:200810722. 28

L. Pentericci, A. Grazian, C. Scarlata, A. Fontana, M. Castellano, E. Giallongo, and E. Vanzella. Physical and morphological properties of z ˜ 3 Lyman break galaxies: dependence on Lyα line emission. A&A, 514:A64, May 2010. doi: 10.1051/0004-6361/200913425. 26

L. Pentericci, E. Vanzella, A. Fontana, M. Castellano, T. Treu, A. Mesinger, M. Dijkstra, A. Grazian, M. Bradač, C. Conselice, S. Cristiani, J. Dunlop, A. Galametz, M. Giavalisco, E. Giallongo, A. Koekemoer, R. McLure, R. Maiolino, D. Paris, and P. Santini. New Observations of z ˜ 7 Galaxies: Evidence for a Patchy Reionization. ApJ, 793:113, October 2014. doi: 10.1088/0004-637X/793/2/113. 42

Patrick Petitjean. QSO Absorption Line Systems. page 24, October 1998. URL `http://arxiv.org/abs/astro-ph/9810418`. 37, 47, 49

M. Pettini and B. E. J. Pagel. [OIII]/[NII] as an abundance indicator at high redshift. MNRAS, 348: L59–L63, March 2004. doi: 10.1111/j.1365-2966.2004.07591.x. 62, 63

M. Pettini, S. A. Rix, C. C. Steidel, K. L. Adelberger, M. P. Hunt, and A. E. Shapley. New Observations of the Interstellar Medium in the Lyman Break Galaxy MS 1512-cB58. ApJ, 569:742–757, April 2002. doi: 10.1086/339355. 48, 51

L. S. Pilyugin. On the oxygen abundance determination in H bt II regions. The problem of the line intensities - oxygen abundance calibration. A&A, 362:325–332, October 2000. 62

L. S. Pilyugin. On the oxygen abundance determination in HII regions. High-metallicity regions. A&A, 369:594–604, April 2001. doi: 10.1051/0004-6361:20010079. 62

L. S. Pilyugin, T. X. Thuan, and J. M. Vílchez. Oxygen abundances in the most oxygen-rich spiral galaxies. MNRAS, 367:1139–1146, April 2006. doi: 10.1111/j.1365-2966.2006.10033.x. 62

L. S. Pilyugin, E. K. Grebel, and L. Mattsson. 'Counterpart' method for abundance determinations in H II regions. MNRAS, 424:2316–2329, August 2012. doi: 10.1111/j.1365-2966.2012.21398.x. 62

N. Pirzkal, S. Malhotra, J. E. Rhoads, and C. Xu. Optical-to-Mid-Infrared Observations of Lyα Galaxies at z˜5 in the Hubble Ultra Deep Field: A Young and Low-Mass Population. ApJ, 667:49–59, September 2007. doi: 10.1086/519485. 28

C. J. Pritchet. The search for primeval galaxies. *Publications of the Astronomical Society of the Pacific*, 106:1052, October 1994. ISSN 0004-6280. doi: 10.1086/133479. URL `http://ucp.uchicago.edu/cgi-bin/resolve?id=doi:10.1086/133479`. 19, 20, 22, 23, 24

J. X. Prochaska, D. Kasen, and K. Rubin. Simple Models of Metal-line Absorption and Emission from Cool Gas Outflows. ApJ, 734:24, June 2011. doi: 10.1088/0004-637X/734/1/24. 54, 71

A. M. Quider, M. Pettini, A. E. Shapley, and C. C. Steidel. The ultraviolet spectrum of the gravitationally lensed galaxy 'the Cosmic Horseshoe': a close-up of a star-forming galaxy at z ˜ 2. MNRAS, 398: 1263–1278, September 2009. doi: 10.1111/j.1365-2966.2009.15234.x. 48, 51, 52

A. Raiter, D. Schaerer, and R. A. E. Fosbury. Predicted UV properties of very metal-poor starburst galaxies. A&A, 523:A64, November 2010. doi: 10.1051/0004-6361/201015236. 18

T. E. Rivera-Thorsen, M. Hayes, G. Östlin, F. Duval, I. Orlitová, A. Verhamme, J. M. Mas-Hesse, D. Schaerer, J. M. Cannon, H. Otí-Floranes, A. Sandberg, L. Guaita, A. Adamo, H. Atek, E. C. Herenz, D. Kunth, P. Laursen, and J. Melinder. The Lyman Alpha Reference Sample. V. The Impact of Neutral ISM Kinematics and Geometry on Lyα Escape. ApJ, 805:14, May 2015. doi: 10.1088/0004-637X/805/1/14. 67, 69

B. D. Savage and K. R. Sembach. The analysis of apparent optical depth profiles for interstellar absorption lines. ApJ, 379:245–259, September 1991. doi: 10.1086/170498. 48, 50

C. Scarlata and N. Panagia. Average outflows properties in ly emitting galaxies. In prep., October 2014. 54, 71

C. Scarlata, J. Colbert, H. I. Teplitz, N. Panagia, M. Hayes, B. Siana, A. Rau, P. Francis, A. Caon, A. Pizzella, and C. Bridge. The Effect of Dust Geometry on the Lyα Output of Galaxies. ApJ, 704: L98–L102, October 2009. doi: 10.1088/0004-637X/704/2/L98. 32

D. Schaerer. The transition from Population III to normal galaxies: Lyalpha and He II emission and the ionising properties of high redshift starburst galaxies. A&A, 397:527–538, January 2003. doi: 10.1051/0004-6361:20021525. 18

U. Seljak, A. Slosar, and P. McDonald. Cosmological parameters from combining the Lyman-α forest with CMB, galaxy clustering and SN constraints. J. Cosmology Astropart. Phys., 10:014, October 2006. doi: 10.1088/1475-7516/2006/10/014. 38

A. E. Shapley, C. C. Steidel, M. Pettini, and K. L. Adelberger. Rest-Frame Ultraviolet Spectra of z˜3 Lyman Break Galaxies. ApJ, 588:65–89, May 2003. doi: 10.1086/373922. 26, 27, 28

Y. Shen, M. A. Strauss, M. Oguri, J. F. Hennawi, X. Fan, G. T. Richards, P. B. Hall, J. E. Gunn, D. P. Schneider, A. S. Szalay, A. R. Thakar, D. E. Vanden Berk, S. F. Anderson, N. A. Bahcall, A. J. Connolly, and G. R. Knapp. Clustering of High-Redshift (z = 2.9) Quasars from the Sloan Digital Sky Survey. AJ, 133:2222–2241, May 2007. doi: 10.1086/513517. 40

E. D. Skillman, R. C. Kennicutt, and P. W. Hodge. Oxygen abundances in nearby dwarf irregular galaxies. ApJ, 347:875–882, December 1989. doi: 10.1086/168178. 62

A. Slosar, A. Font-Ribera, M. M. Pieri, J. Rich, J.-M. Le Goff, É. Aubourg, J. Brinkmann, N. Busca, B. Carithers, R. Charlassier, M. Cortês, R. Croft, K. S. Dawson, D. Eisenstein, J.-C. Hamilton, S. Ho, K.-G. Lee, R. Lupton, P. McDonald, B. Medolin, D. Muna, J. Miralda-Escudé, A. D. Myers, R. C. Nichol, N. Palanque-Delabrouille, I. Pâris, P. Petitjean, Y. Piškur, E. Rollinde, N. P. Ross, D. J. Schlegel, D. P. Schneider, E. Sheldon, B. A. Weaver, D. H. Weinberg, C. Yeche, and D. G. York. The Lyman-α forest in three dimensions: measurements of large scale flux correlations from BOSS 1st-year data. J. Cosmology Astropart. Phys., 9:001, September 2011. doi: 10.1088/1475-7516/2011/09/001. 38

D. P. Stark, R. S. Ellis, S. Charlot, J. Chevallard, M. Tang, S. Belli, A. Zitrin, R. Mainali, J. Gutkin, A. Vidal-García, R. Bouwens, and P. Oesch. Lyα and CIII] Emission in z = 7 - 9 Galaxies: Accelerated Reionization Around Luminous Star Forming Systems? MNRAS, September 2016. doi: 10.1093/mnras/stw2233. 42

C. Steidel, M. Giavalisco, M. Pettini, M. Dickinson, and K. Adelberger. Spectroscopic Confirmation of a Population of Normal Star-Forming Galaxies at Redshifts z>3. page 12, February 1996. doi: 10.1086/310029. URL `http://arxiv.org/abs/astro-ph/9602024`. 24, 25

C. C. Steidel and D. Hamilton. Deep imaging of high redshift QSO fields below the Lyman limit. II - Number counts and colors of field galaxies. AJ, 105:2017–2030, June 1993. doi: 10.1086/116579. 24

C. C. Steidel, K. L. Adelberger, M. Giavalisco, M. Dickinson, and M. Pettini. Lyman-Break Galaxies at z˜4 and the Evolution of the Ultraviolet Luminosity Density at High Redshift. ApJ, 519:1–17, July 1999. doi: 10.1086/307363. 26

C. C. Steidel, K. L. Adelberger, A. E. Shapley, M. Pettini, M. Dickinson, and M. Giavalisco. Lyα Imaging of a Proto-Cluster Region at <z>=3.09. ApJ, 532:170–182, March 2000. doi: 10.1086/308568. 18

C. C. Steidel, K. L. Adelberger, A. E. Shapley, M. Pettini, M. Dickinson, and M. Giavalisco. Lyman Break Galaxies at Redshift z ˜ 3: Survey Description and Full Data Set. ApJ, 592:728–754, August 2003. doi: 10.1086/375772. 26

T. Storchi-Bergmann, D. Calzetti, and A. L. Kinney. Ultraviolet to near-infrared spectral distributions of star-forming galaxies: Metallicity and age effects. ApJ, 429:572–581, July 1994. doi: 10.1086/174345. 62

G. Tenorio-Tagle, S. A. Silich, D. Kunth, E. Terlevich, and R. Terlevich. The evolution of superbubbles and the detection of Lyα in star-forming galaxies. MNRAS, 309:332–342, October 1999. doi: 10.1046/j.1365-8711.1999.02809.x. 33, 71

Thorsten Tepper Garcia. Voigt profile fitting to quasar absorption lines: an analytic approximation to the Voigt-Hjerting function. *Monthly Notices of the Royal Astronomical Society*, 369(4):2025, 2006. doi: 10.1111/j.1365-2966.2006.10450.x. 47

E. Terlevich, A. I. Diaz, R. Terlevich, and M. L. G. Vargas. New detections of Ly-alpha emission in young galaxies. MNRAS, 260:3–8, January 1993. 26

C. van Breukelen, M. J. Jarvis, and B. P. Venemans. The luminosity function of Lyα emitters at 2.3 z 4.6 from integral-field spectroscopy*. MNRAS, 359:895–905, May 2005. doi: 10.1111/j.1365-2966.2005.08916.x. 20

B. P. Venemans, J. D. Kurk, G. K. Miley, H. J. A. Röttgering, W. van Breugel, C. L. Carilli, C. De Breuck, H. Ford, T. Heckman, P. McCarthy, and L. Pentericci. The Most Distant Structure of Galaxies Known: A Protocluster at z=4.1. ApJ, 569:L11–L14, April 2002. doi: 10.1086/340563. 15

B. P. Venemans, H. J. A. Röttgering, G. K. Miley, J. D. Kurk, C. De Breuck, R. A. Overzier, W. J. M. van Breugel, C. L. Carilli, H. Ford, T. Heckman, L. Pentericci, and P. McCarthy. Properties of Lyα emitters around the radio galaxy MRC 0316 257′. A&A, 431:793–812, March 2005. doi: 10.1051/0004-6361:20042038. 28

A. Verhamme, D. Schaerer, and A. Maselli. 3D Lyα radiation transfer. I. Understanding Lyα line profile morphologies. A&A, 460:397–413, December 2006. doi: 10.1051/0004-6361:20065554. 34, 35, 69

A. Verhamme, D. Schaerer, H. Atek, and C. Tapken. 3D Lyα radiation transfer. III. Constraints on gas and stellar properties of z ˜ 3 Lyman break galaxies (LBG) and implications for high-z LBGs and Lyα emitters. A&A, 491:89–111, November 2008. doi: 10.1051/0004-6361:200809648. 34

A. Verhamme, Y. Dubois, J. Blaizot, T. Garel, R. Bacon, J. Devriendt, B. Guiderdoni, and A. Slyz. Lyman-α emission properties of simulated galaxies: interstellar medium structure and inclination effects. A&A, 546:A111, October 2012. doi: 10.1051/0004-6361/201218783. 28, 35

A. Verhamme, I. Orlitová, D. Schaerer, and M. Hayes. Using Lyman-α to detect galaxies that leak Lyman continuum. A&A, 578:A7, June 2015. doi: 10.1051/0004-6361/201423978. 43, 73

D. H. Weinberg, R. Davé, N. Katz, and J. A. Kollmeier. The Lyman-α Forest as a Cosmological Tool. In S. H. Holt and C. S. Reynolds, editors, *The Emergence of Cosmic Structure*, volume 666 of *American Institute of Physics Conference Series*, pages 157–169, May 2003. doi: 10.1063/1.1581786. 38

L. Wisotzki, R. Bacon, J. Blaizot, J. Brinchmann, E. C. Herenz, J. Schaye, N. Bouché, S. Cantalupo, T. Contini, C. M. Carollo, J. Caruana, J.-B. Courbot, E. Emsellem, S. Kamann, J. Kerutt, F. Leclercq, S. J. Lilly, V. Patrício, C. Sandin, M. Steinmetz, L. A. Straka, T. Urrutia, A. Verhamme, P. M. Weilbacher, and M. Wendt. Extended Lyman α haloes around individual high-redshift galaxies revealed by MUSE. A&A, 587:A98, March 2016. doi: 10.1051/0004-6361/201527384. 21

A. Wofford, C. Leitherer, and J. Salzer. Lyα Escape from z ˜ 0.03 Star-forming Galaxies: The Dominant Role of Outflows. ApJ, 765:118, March 2013. doi: 10.1088/0004-637X/765/2/118. 27, 71

A. M. Wolfe. New evidence from the Lyman-alpha forest concerning the formation of galaxies. *Royal Society of London Philosophical Transactions Series A*, 320:503–515, December 1986. doi: 10.1098/rsta.1986.0132. 37

S. Y. Yin, Y. C. Liang, F. Hammer, J. Brinchmann, B. Zhang, L. C. Deng, and H. Flores. Empirical strong-line oxygen abundance calibrations from galaxies with electron-temperature measurements. A&A, 462:535–546, February 2007. doi: 10.1051/0004-6361:20065798. 62, 63